ANL-76-72

ANL-76-72

PHYSICS OF REACTOR SAFETY

Quarterly Report

January—March 1976

ARGONNE NATIONAL LABORATORY, ARGONNE, ILLINOIS

Prepared for the U. S. NUCLEAR REGULATORY COMMISSION
under Contract W-31-109-Eng-38

Printed in the United States of America
Available from
National Technical Information Service
U. S. Department of Commerce
5285 Port Royal Road
Springfield, Virginia 22161
Price: Printed Copy $4.00; Microfiche $2.25

Distribution Category:
Advanced Reactor Safety
Research—Fast Reactors
(NRC-7)

ANL-76-72

ARGONNE NATIONAL LABORATORY
9700 South Cass Avenue
Argonne, Illinois 60439

PHYSICS OF REACTOR SAFETY

Quarterly Report
January—March 1976

Applied Physics Division

Work performed for the
Division of Reactor Safety Research
U. S. Nuclear Regulatory Commission

Previous reports in this series

ANL-75-31	January—March 1975
ANL-75-67	April—June 1975
ANL-76-6	July—September 1975
ANL-76-13	October—December 1975

TABLE OF CONTENTS

TABLE OF CONTENTS

LIST OF FIGURES

LIST OF TABLES

PHYSICS OF REACTOR SAFETY

Quarterly Report
January--March 1976

I. ABSTRACT

This quarterly progress report summarizes work done in Argonne National Laboratory's Applied Physics Division for the Division of Reactor Safety Research of the U.S. Nuclear Regulatory Commission during the months of January-March 1976. It includes reports on reactor safety research and technical coordination of the RSR safety analysis program by members of the Reactor Safety Appraisals Group, Monte Carlo analysis of safety-related critical assembly experiments by members of the Theoretical Fast Reactor Physics Group, and planning of DEMO safety-related critical experiments by members of the Zero Power Reactor (ZPR) Planning and Experiments Group.

TECHNICAL COORDINATION - FAST REACTOR SAFETY ANALYSIS (A2015)

II. SUMMARY

Studies of double-ended pipe rupture accidents with scram have been made for the CRBR using the DEMO code. It was found that coolant boiling will occur in the DEMO model "hot" channel, which includes engineering hot-channel factors, about 1.4 seconds after a double-ended rupture of the inlet nozzle. The coolant flow through the core falls to 35 to 40% of the original value in 0.2 seconds in this case. As the rupture moves away from the inlet nozzle the flow reduction quickly decreases and boiling conditions no longer occur. Comparison with SAS3A calculations for the same flow reduction and scram reactivity insertion rate indicate that DEMO is giving maximum coolant temperatures about 40°C higher than those from SAS3A. Parametric studies have been made with SAS3A of the effect of pin peak power density, initial coolant flow rate, and fuel-clad gap conductance on the maximum coolant temperature attained, with boiling assumed suppressed, for a double-ended rupture at the inlet nozzle.

It was determined that 14 cycles would be needed to attain complete equilibrium cycle conditions in the CRBR, corresponding to a number of years of operation, so that some consideration of the behavior of reactivity coefficients and power distribution during the approach to equilibrium conditions seems appropriate. Improved calculations of power distribution and reactivity coefficients have been made for the beginning-of-equilibrium cycle case in the CRBR. In these calculations stagewise burnt up fuel compositions rather than stage-homogenizing compositions were used. An

R-Z model was used for reactivity coefficient calculations and a 2D triangular mesh model was used for power distribution calculations. Core subassembly power factors were found to range from 3.2% higher to 4.5% lower than the values reported in the CRBR PSAR. There is considerable sensitivity of the power distribution in the outer part of the core to assumptions about fuel management and composition regions in the radial blanket, and there appears to be some inconsistency between WARD and us in this respect. Large skewing of the axial power distribution was found to occur from partially-inserted control rods, using an R-Z model.

Reactivity coefficients and power distribution calculations have been made for the end-of-equilibrium cycle for the CRBR using stage-and-height-dependent compositions. Values of the Doppler constant Tdk/dT were found to decrease with increasing temperatures, and were slightly lower than values obtained by the CRBR project for somewhat different temperature assumptions.

Streaming effects in the sodium void effect in the inner core of the CRBR were evaluated by using directional diffusion coefficients calculated by Benoist's theory. The positive effect was reduced by only 7% from the increase in leakage component, indicating that the streaming effect is small in the CRBR pin geometry.

The EPIC fuel-coolant interaction code is operational and yields stable results for an unvoided channel and a clad rip only one node long. Work is not yet complete for handling a partially voided channel and multiple cell rips. Comparison with the PLUTO1 code showed that velocities in the fuel pin cavity next to the clad failure node are about twice as high as PLUTO's during the first 5-10 multi-seconds of the transient and the mass of fuel ejected from the pin into the channel in EPIC is about 25% higher than that in PLUTO in this time period. The velocities of the liquid sodium slugs in the coolant channel are 60-70% higher in EPIC than in PLUTO, almost all of the first two differences can be explained by the different numerical techniques used in the two codes for the hydrodynamics in the fuel pin. In PLUTO it was necessary to introduce an artificial viscosity to stabilize the solution, a strategy not necessary in EPIC, and this was found to have a considerable effect on the results. Use of the EPIC numerical techniques in PLUTO largely eliminated the first two differences mentioned. The differences in coolant liquid slug velocities are apparently caused by different numerical models in the coolant channel. Use of cell-edge velocities (a better technique, used in EPIC) instead of the cell-centered velocities used in PLUTO eliminated about half the discrepancy.

The approximate incompressible region treatment developed for boiling fuel/steel pools appears to be stable and to converge well, and allows the effect of a local pressure pulse to be followed much farther than was previously possible. However, this technique appears to cause a loss of kinetic energy from the fluid. To what extent this effect corresponds to physical reality is not yet clear. Uncertainty in this point is hindering the assessment of the effect of fuel-steel heat transfer on disassembly work energy.

Assistance has been given to NRC in defining the format and schedule for a meeting of RSR principal investigators to be held in April.

A recent interesting development in critical experiment interpretation is the discovery that C/E ratios for off-center sodium voiding experiments in ZPPR 5 are much more consistent if directional diffusion coefficients based on Benoist's theory are used. Streaming appears to increase the leakage component by 40 to 50%, and C/E is fairly consistently equal to 1.2 for the radially dependent sodium-voiding measurements, consistent with an error in the conversion from inhours to %k. Reexamination of the FTR-EMC sodium voiding measurements indicates that they, too, can be satisfactorily interpreted by a streaming correction of 40% to 50% in the leakage component and a consistent C/E of about 1.2. This suggests that no bias should be applied to FTR sodium voiding calculations to force agreement with the experiments.

A meeting was held at Argonne on April 5th and 6th to attempt to achieve a consensus that recriticality is no longer a live issue for LMFBR's, but this goal was not attained. A key uncertainty is whether or not a stable crust of frozen fuel will form at the bottom and sides of a boiling fuel/steel pool. Such a crust would inhibit heat transfer and allowing the pool to stay boiled up at decay power, making collapse of the pool and recriticality difficult. There is a great lack of experimental information dealing with this question and with others such as the transition of a melting core to a boiling pool, the behavior of boiling pools with two materials, basic material size and distribution functions, and potential modes of recompaction. This lack of information hampers modeling efforts in the area of recriticality. Although the potential for an energetic recriticality seems small, it is difficult to demonstrate this conclusively at present.

III. STUDY OF BASIC PROBLEMS IN ACCIDENT ANALYSIS

A. Initiating Condition Variations

1. Pipe Rupture Studies for the CRBR Using DEMO and SAS (H. H. Hummel and Kalimullah)

Double-ended pipe rupture (in one of the 3 loops) calculations have been carried out for the Clinch River Breeder Reactor[1] with the DEMO code[2] for varying break locations and scram times. Flow through the core following a break at the core inlet coolant nozzle falls in about 0.2 sec to between 0.35 and 0.40 of the original flow (Fig. 1). Trip on flux/$\sqrt{\text{inlet plenum pressure}}$ occurs at 0.633 sec. Because of pump trip, after about 2.5 sec the flow coasts down to pony motor speed (0.1 of normal) in about 10 seconds. Pressure in the inlet plenum is sustained in the first 0.2 sec largely by the inertial head of fluid being accelerated out of the break. After this time the friction head of this fluid is the dominant term.

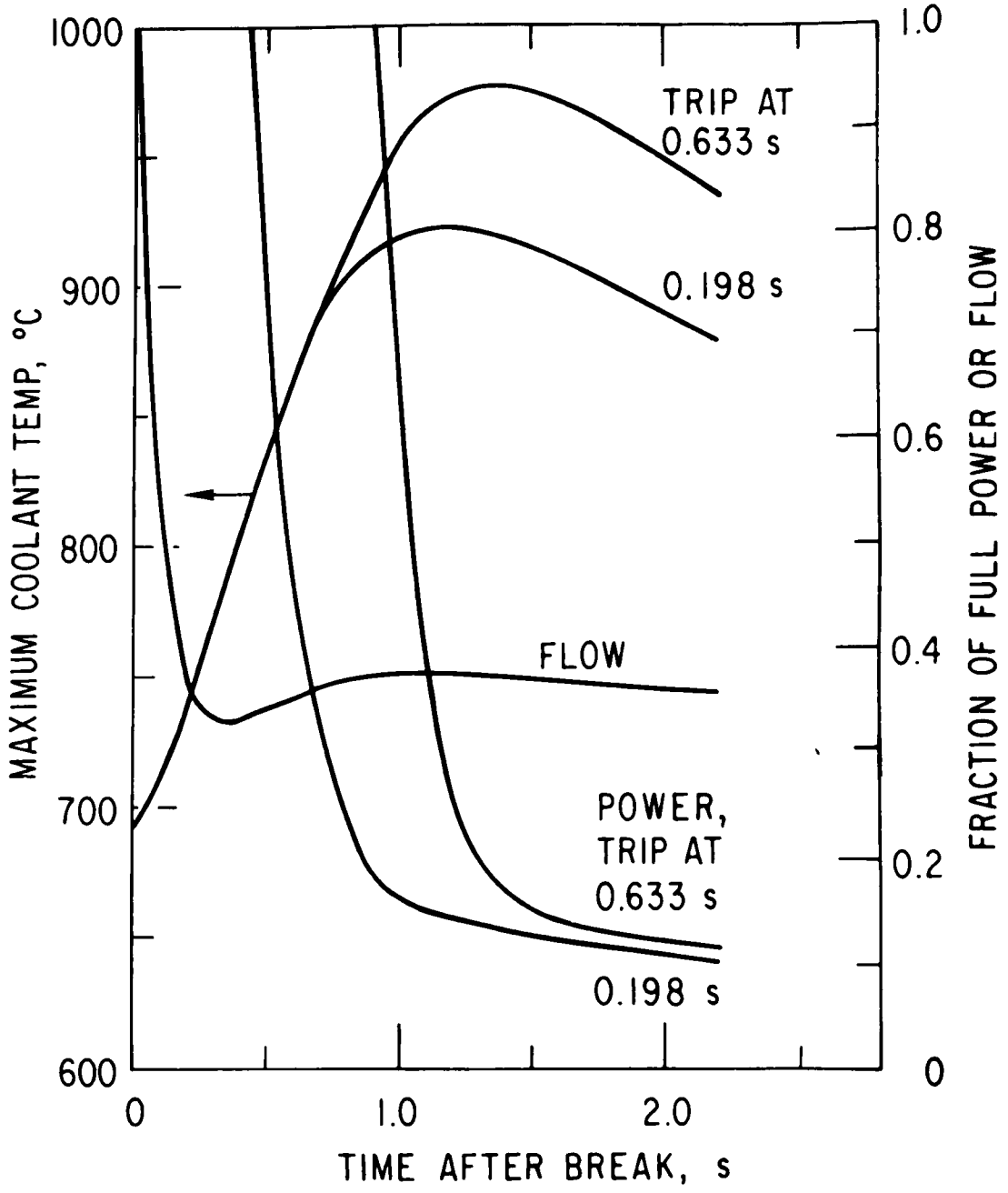

Fig. 1. Flow Reduction, Power, and Maximum Coolant Temperature as a Function of Time for a Double-Ended Pipe Rupture of the CRBR Inlet Nozzle. Boiling is Assumed Suppressed. ANL Neg. No. 116-76-82.

As shown in Fig. 1, the coolant temperature in the core goes through a maximum in 1.2 to 1.4 seconds following a break at the inlet nozzle, assuming that boiling conditions have not been attained or that boiling is suppressed. The reactor guard vessel is irrelevant to the question of boiling because liquid sodium does not even cover the pipe opening until about 5 seconds after the break occurs. Boiling does occur in the DEMO model "hot" channel[2] (with engineering hot channel factors of 1.58 for power and 1.17 for flow compared to an average channel) for a break at the inlet nozzle, but not in the "peak" channel, which includes nuclear design peaking factors. The hot channel factors for power and flow for the peak channel were 1.36 and 1.06 respectively. The factors used in this calculation were those assumed in the DEMO code sample problem and do not necessarily agree with those in the CRBR PSAR.[1]

As the rupture moves away from the inlet nozzle the rate of flow decay in the first seconds after a break is greatly retarded because of the larger inertial head associated with the greater length of fluid. For a break halfway between the inlet nozzle and the IHX the inertial head remains significant for about 1.5 seconds after the break. There is also a static head because of elevation of the pipe at this point. Flow through the reactor vessel falls to about 0.4 of the original value in 2.5 seconds and to 0.25 of the original value in 8 seconds. Boiling in the DEMO hot channel does not occur under these conditions.

In order to obtain more detailed temperature calculations in the reactor core than are provided by the DEMO code, flow reduction and scram reactivity insertion rates from DEMO for rupture at the inlet nozzle were inserted into the SAS 3A code. It was concluded that for consistent assumptions maximum coolant temperatures calculated by SAS were about 40°C less than those calculated by DEMO. Balancing this is the fact that the fuel-clad gap conductance assumed for the DEMO hot channel was about 0.6 watts/cm^2-C°, which may be somewhat optimistic. A reasonable lower limit is about 0.3 watts/cm^2-C°, which corresponds to an increase in maximum coolant temperature of 30°C to 50°C (assuming that boiling is suppressed if it would otherwise occur). Another result of parametric studies (Fig. 2) is that an increase of 16% in maximum pin power density from 11.09 kw/ft, the peak channel value, to 12.88 kw/ft, the hot channel value, increases the maximum coolant temperature by 80°C to 90°C. A 16% decrease in initial coolant flow rate increases the maximum coolant temperature by 50°C to 60°C. An earlier protective system trip at 0.198 sec instead of 0.633 sec reduces the maximum coolant temperature by 40°C to 50°C.

The SAS calculations indicate that for a rupture at the inlet nozzel and trip at 0.633 sec the boiling temperature, 950°C at the existing coolant pressure, is exceeded for the DEMO model hot channel with a gap conductance of 0.6 watts/cm^2-C° by about 30°C, with boiling assumed suppressed. This indicates that to prevent boiling either the power density would have to be lowered by at least 6% or the coolant flow rate would have to be increased by at least 8%. Maintaining the coolant flow rate for about 3 seconds after the rupture at 40 to 45% of the initial value followed by a gradual decrease should prevent boiling in the hot channel. For a gap conductance of 0.3 watts/cm^2-°C the power density would have to be lowered by about 13% or the flow rate increased by about 20%.

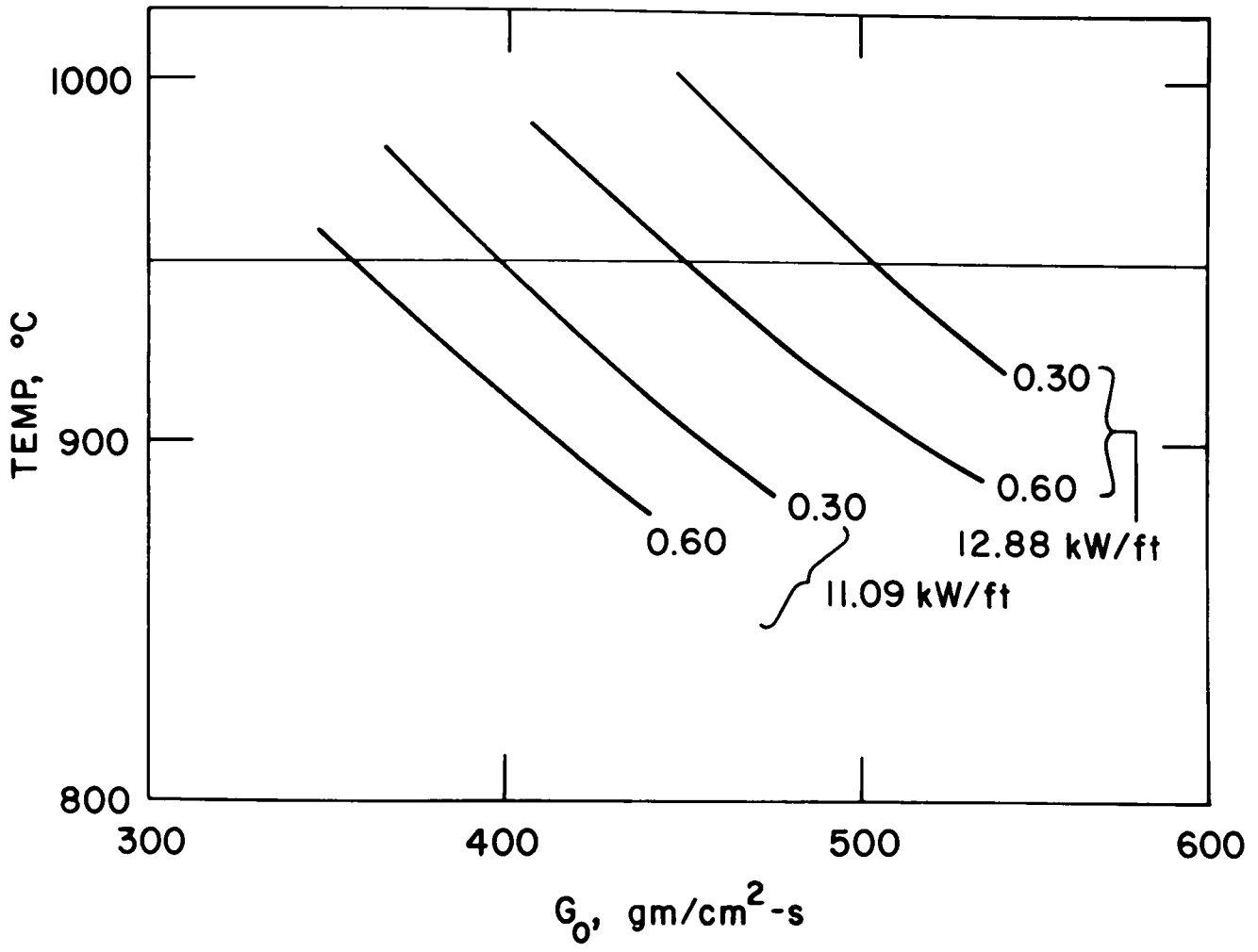

Fig. 2. Relation of Maximum Coolant Temperature (with Boiling Assumed Suppressed), Coolant Velocity, Maximum Pin Power Density, and Gap-Conductance (watts/cm^2-°C) for a Double-Ended Pipe Rupture at the CRBR Inlet Nozzle with Trip at 0.633 sec. ANL Neg. No. 116-76-78.

2. Power Distribution in the Clinch River Breeder Reactor (CRBR) at the Beginning of Equilibrium Cycle (BOEC) (Kalimullah and H. H. Hummel)

The present calculations of power and reactivity distributions are improved over those reported in Ref. 3 in that stagewise burnup fuel composition rather than the stage-homogenized compositions were used. For burnup and reactivity coefficients this was accomplished in R-Z geometry by using adjacent annular regions for the separate stages; for power distribution the actual subassembly layout was used in a 2 D triangular mesh geometry. The effect of partially inserted control rods in skewing the axial distribution of power and reactivity coefficients has also been studied.

An analysis has been made of the approach to the equilibrium cycle using the core and radial blanket fuel management for the initial cycles indicated in the CRBR PSAR, Fig. 4.3-3, and described in some detail in Ref. 4. It was found that cycle 8 is the earliest that appears to have subassembly burnups corresponding to the equilibrium cycle and that cycle 11 is the earliest for which complete equilibrium cycle fluxes and compositions would be achieved in the core, which has a 3-cycle residence time. For the radial blanket, which has a 6-cycle residence time, complete equilibrium would not be achieved until cycle 14. The present calculation of power and reactivity coefficient distribution have been based on composition for the beginning of cycle 14. The first cycle is 128 days, the second 200 days, and the third and succeeding are 274 days. It thus appears that it will be a number of years before equilibrium cycle conditions are achieved, if they ever are, because a different core may be installed after a few years. Some consideration thus needs to be given to the behavior of reactivity coefficients and power distribution during the approach to equilibrium cycle, although the safety significance of these changes may not be very large.

In the R-Z model burnup and reactivity-coefficient calculations, four equal-height axial segments were used over the core half-height and two equal segments were used for the axial blanket. For the 2 D triangular mesh calculations the core axial segments were homogenized. Cross sections were generated in 27 groups for four regions (inner core, outer core, radial blanket, and reflector) for various temperatures and with sodium both present and voided, using ENDF/B-III data in the MC^2-2 codes.[5,6]

In the 2 D triangular mesh calculations the B_4C volume fractions of the control rods (natural enrichment for the central rod and 50% for the others) have been reduced from the actual values to account for their partial insertion (2/3 for the central rod and the six rods at the flats of run 7 (bank 2), 1/3 for the six rods at the corner of run 7 (bank 3)). Relative worths for the various rod banks were calculated for the fully-inserted rod in the extrapolated base height triangular mesh model, and the fraction of this worth for the partially-inserted rod was calculated from this using a chopped-cosine flux and adjoint weighting. The total worth of all three banks was set at -5.88%k, needed to make the system critical at the beginning of cycle 14. A concentration search was thus conducted for each rod bank to find the B_4C volume fraction that would

give this fractional worth. Volume fractions of B_4C arrived at in this way were 0.1888, 0.1649, and 0.0425 respectively for the central rod, bank 2, and bank 3, compared to an actual volume fraction of 0.3390. The corresponding bank worths were -0.636, -4.093, and -1.152%k respectively. These adjusted B_4C volume fractions are reduced more than would be expected from the partial insertion of the rods because of the reduced spatial self-shielding at the lower concentrations.

Core subassembly power factors calculated with the 2 D triangular mesh model with B_4C concentrations obtained in this way range from 3.2% higher to 4.5% lower than the values reported in the PSAR[1], Fig. 4.3-7, most of the larger differences being in the outer core subassemblies. Total radial blanket power has been found to be 57.6 MW (59.0 MW from the 2-D R-Z calculation described below) compared to 76.1 MW reported in the PSAR Table 4.3-7. These differences are due to (a) the inaccuracies in the present radial blanket burnt fuel compositions arising from the use of only one region in the radial direction in the R-Z model used for burnup calculation and (b) the use of an incorrect radial blanket subassembly-burnup pattern[7] (different from any of the six patterns it takes during its equilibrium operation) for the calculation the power factors reported in the PSAR Fig. 4.3-7. The power factors of core subassemblies are fairly sensitive to the detailed composition of the radial blanket. If the detailed stage-wise burnup compositions used in the present calculations in the radial blanket were homogenized and used in all the blanket subassemblies, the radial blanket power would increase to about 72.0 MW, the power factors of subassemblies in row 2 of the inner core would decrease by about 4%, and those of outer core subassemblies increase by a few percent. The reason is that the fissile isotope content of the newer radial blanket subassemblies adjacent to the outer core is considerably lower than that of the older subassemblies in the outer rows of the blanket. Homogenization of these subassemblies is equivalent to moving fissile isotopes radially inwards, and this tilts the overall radial shape of the neutron flux (and hence power) such that it increases at larger core radii and decreases at smaller radii (as if a bank of absorber rods were withdrawn at the core-blanket interface).

In order to calculate the axial distribution of power a fairly detailed full-height R-Z model of the Clinch River Breeder Reactor (CRBR) was constructed for the beginning of cycle 14. The core subassemblies were represented by 25 annuli, the radial blanket subassemblies by 3 and the control banks 2 and 3 were split respectively into 2 and 3 annuli such that the model maintains as far as practicable (a) the radial distances of subassemblies from the reactor axis, (b) the relative locations of fuel subassemblies of varying burnups, and (c) the relative location of fuel and control subassemblies. The axial variation of fuel composition in the burnt core and radial blanket subassemblies (determined for six axial segments over the half height of the reactor as described above) was taken into account in the model except that the compositions for the two segments nearest to the core midplane were homogenized. For these two compositions, the maximum difference between ^{239}Pu atom densities was about 1.2% for various core subassemblies (5.5% for various radial blanket subassemblies), the maximum difference between ^{238}U atom densities about 0.7% for the core (0.5% for radial blanket), and the maximum difference between atom densities of

fission products was about 6% for the core (13% for radial blanket). The axial and radial reflectors were of neutronically infinite thicknesses in the model. The central control rod (bank 1) and the six rods of bank 2 were inserted two-thirds and the six rods of bank 3 one-third into the core, some portion of the absorber rods extending into the upper axial reflector. The volume fractions of B_4C for each of the three control banks were adjusted to the normalized worths discussed above, i.e., 0.636, 4.093 and 1.152% Δk, by carrying out a separate concentration search for each control bank using R-Z diffusion theory. The volume fractions of natural B_4C for the central rod and 50% enriched B_4C for control banks 2 and 3 were found to be 0.2501, 0.1621 and 0.1243 compared to the actual volume fraction of 0.3390. These adjusted volume fractions of B_4C are lower than the actual value mainly because of (a) the reduction in spatial self-shielding arising from modeling discrete subassemblies into annuli, (b) the overestimation of central rod worths by R-Z geometry diffusion theory calculation[8] (the volume fraction of 0.3390 was based on transport theory).

Using these adjusted B_4C volume fractions the flux and power distribution in the critical reactor was calculated for the beginning of cycle 14. The maximum (in row 7 subassemblies) and the minimum (in row 2 subassemblies) axial power shape skewness [(power density at core bottom)/(power density at core top) minus 1] are about 75% and 27%, compared to 20% subassembly-independent skewness reported in the PSAR Fig. 4.3-9. The skewness adjacent to the central control rod is nearly 46%. The region wise total powers are found to

Inner core	= 508.5 MW,
Outer core	= 376.0 MW,
Lower axial blanket	= 19.4 MW,
Upper axial blanket	= 11.8 MW,
Radial blanket	= 59.0 MW,

3. Reactivity Calculations for the CRBR at End-of-Equilibrium-Cycle (EOEC) for SAS-3A Analysis (P. H. Kier)

Reactivity coefficients were computed for EOEC conditions using the full reactor, R-Z model and the 27-group cross section set based on ENDF/B-III data burnup calculations were run to obtain stage-and-height-dependent compositions. In the core these stage-and-height-dependent compositions were used while in the radial blanket compositions were stage-homogenized and height-dependent. Diffusion theory calculations were run to obtain real and adjoint flux distributions for six cases: the system at 1100K, 2200K, and 4400K with sodium in and with sodium voided from all regions except the control rod channels and the reflector. These fluxes were used in first-order perturbation theory computations of the distribution of the sodium void worth, the Doppler coefficient, the steel reactivity worth and the core fuel worth. Also, the power distribution was computed. These distributions were processed into a format suitable for input to SAS-3A.

The results of these computations are summarized in Tables I and II. The steel worths and core fuel worths were computed for all six cases to provide information on the sensitivity of these quantities to temperature

Table I. Steel Worth, Fuel Worth, Power, and Sodium Void by Region

Quantity	Fluxes Sodium	Temp. °K	Cross Sections at	Inner Core	Outer Core	Lower Axial Blanket	Upper Axial Blanket	Radial Blanket	Total
Steel Worth $\Delta k/k \times 10^3$	in	1100	1100	-42.45	-6.23	1.71	2.43	3.05	-41.49
	in	2200	2200	-43.05	-6.35	1.71	2.40	3.01	-42.28
	in	4400	2200	-43.69	-6.49	1.69	2.36	2.98	-43.15
	void	1100	1100	-40.84	-3.70	3.22	3.95	4.01	-33.37
	void	2200	2200	-40.86	-3.76	3.12	3.84	3.89	-33.80
	void	4400	2200	-41.51	-3.89	3.05	3.78	3.82	-34.74
Fuel Worth $\Delta k/k \times 10^3$	in	1100	1100	196.95	160.54	25.88	20.45		403.83
	in	2200	2200	198.96	162.04	25.73	20.46		407.21
	in	4400	2200	203.39	164.40	25.84	20.59		414.22
	void	1100	1100	209.82	169.10	32.48	26.34		437.74
	void	2200	2200	211.14	169.98	32.33	26.34		439.79
	void	4400	2200	213.89	171.35	32.36	26.41		444.01
Power, MW	in	1100	1100	465.8	365.8	26.7	20.2	96.5	975
Sodium Void $\Delta k/k \times 10^3$	in	1100	1100	14.83	0.15	-0.86	-0.87	-1.18	12.07

Table II. Doppler Coefficient $\alpha = \frac{Tdk}{dT} \times 10^4$

Case	Flux Sodium	Flux Temp.	Cross Section change, °K	Inner Core	Outer Core	Lower Axial Blanket	Upper Axial Blanket	Radial Blanket	Total
1	in	1100	1100 → 2200	39.52	13.12	6.81	3.18	12.46	75.09
2	in	2200	2200 → 4400	36.60	11.86	6.52	3.04	11.24	69.26
3	in	4400	2200 → 4400	34.02	11.01	5.55	2.68	9.50	62.76
4	in	*	2200 → 4400	35.31	11.43	6.03	2.86	10.37	66.00
5	voided	1100	1100 → 2200	24.97	8.32	5.47	2.53	10.96	52.25
6	voided	2200	2200 → 4400	22.20	7.22	5.06	2.32	9.65	46.45
7	voided	4400	2200 → 4400	20.77	6.73	4.34	2.07	8.25	42.16
8	voided	**	2200 → 4400	21.48	6.97	4.70	2.19	8.95	44.29

* average of cases 3 and 4

** average of cases 6 and 7

and the absence of sodium. It is seen that the steel worths and core fuel worths are relatively insensitive to temperature. The steel worth exhibits a significant dependence upon the presence of sodium. The decrease in the negativity can be explained in terms of the harder neutron spectrum when sodium is voided. Hardening of the neutron spectrum augments the positive leakage term relative to the negative capture term in the perturbation theory formulation of reactivity. In the inner core, where flux gradients are smaller than in other regions the increase in the leakage term is less pronounced so that the change in steel worth with sodium voiding is relatively smaller. The hardened neutron spectrum in the sodium voided system causes an increase in the core fuel worth by augmenting the positive fission source term relative to the negative absorption term. However, this effect is mitigated by the reduction in microscopic cross sections of the fertile and fissile nuclides from increased shielding when sodium is absent.

Table II gives the Doppler coefficient for eight cases. The Doppler decreases with increasing temperature and sodium voiding from the spectrum hardening out of the energy range where capture cross sections increase with temperature. It also decreases with temperature because the capture cross section change per unit temperature change decreases with increasing temperature. The results of these calculations indicate that the Doppler effect decreases more rapidly with temperature than an inverse temperature dependence would predict.

When we take the average of the Doppler coefficient computed with cross section changes from 2200 to 4400 K with fluxes computed for 2200 K and with fluxes computed for 4400 K, cases 4 and 8, there results a Doppler coefficient for the ten channels that are input to SAS-3A 7% lower than that obtained using a computed temperature distribution in the reactor and a uniform increase in temperature of 1000 K above that base temperature distribution[9].

4. Effect of Streaming on the Sodium Void Worth in the Inner Core of the CRBR at Beginning-of-Life (BOL) (P. H. Kier)

An exploratory set of calculations was performed to assess the importance of neutron streaming along voided sodium channels on the reactivity worth of sodium. Three R-Z, half-reactor diffusion theory calculations of eigenvalue were run. In one calculation sodium was present in all regions of the reactor; in the other two calculations sodium was voided from the inner core. In one of the voided calculations, the group diffusion coefficients for the inner core were based on the usual assumption of a homogenized cell. The other voided calculations used directional diffusion coefficients computed according to Benoist's formulation[10] by a Monte Carlo code[11] that treats a two-region circularized cell in which the fuel pin and clad are homogenized together and in which the coolant annulus is empty. The result of the calculations was that the increase in the multiplication constant resulting from removal of sodium from the inner core was reduced by 7% when streaming effects were included when computing the diffusion coefficients for the sodium-voided region. Although this study is not definitive, it indicates that the neglect of streaming is not an overwhelming source of systematic error in our calculation of the sodium void effect.

5. Calculation of Subassembly Power Factors for the CRBR at End of Equilibrium Cycle (EOEC) (P. H. Kier)

Triangular mesh 2-D diffusion calculations were run to obtain subassembly power factors for the CRBR at the end of six successive equilibrium cycles, Cycles 8 through 13. The power factor is defined as the ratio of the average power in the subassembly to the average power in the zone where the zone is either the core or the radial blanket. Each subassembly in the core and the radial blanket was assigned the appropriate axially-averaged, stage-dependent composition. Cycles 8 and 11, cycles 9 and 12, and cycles 10 and 13 had identical composition-assembly assignments in the core but different assignments in the radial blanket. The power factors in the core were found to be generally insensitive to the composition-subassembly assignments in the radial blanket. For a configuration that simulated that given in the PSAR[1] significant differences in power factors were obtained in the outer row of the core and the radial blanket with these calculations yielding smaller power factors in the outer row of the core and a smaller power generation in the radial blanket. We are attempting to determine the source of the discrepancy. We suspect that we have underestimated the burnup of fuel in the radial blanket that has been exposed less than six cycles by treating the radial blanket as one region radially in the burnup calculations. These calculations are being rerun with the radial blanket divided into six radial regions to better represent burnup there.

B. Model Studies

1. Development of EPIC Fuel-Coolant-Interaction Computer Code (P. A. Pizzica and P. B. Abramson)

The EPIC (Eulerian-Particle-In-Cell) fuel-coolant interaction computer code is operational and the calculation is stable for the case of an unvoided channel and a pin failure only one Eulerian node long. Both the cases of ejecting fuel into a partially voided channel and of ejecting through a failure more than one Eulerian node long are stable out to a few milliseconds before encountering difficulties (no major effort has yet been expended on these areas).

The particle-in-cell technique used for tracking the fuel particles in the channel is working well. This allows a detailed picture of fuel motion in the channel at the cost of much computer time (which is a function of the number of particles tracked). The technique is as follows: The pressure equilibration model for ejection of fuel[12] from the molten fuel cavity in the fuel pin determines how much fuel must be ejected from the pin into the channel in order to make the pressure equal in the ejecting pin node and in the channel node in front of the rupture. The user inputs approximately how much mass of fuel constitutes one fuel marker "particle" by specifying the number of actual fuel particles (i.e. the particle size used in the heat transfer and drag calculations) per master particle (actually a group of fuel particles). The total mass ejected is thus divided into a number of marker particles. The mass of each group is accounted for exactly. Each particle is placed at a random location in front of the rupture and is assigned a zero velocity. A drag on the

particle from the medium and a pressure gradient across the medium which accelerates the particles are then calculated. In this manner, the mass, velocity and location of each marker particle is tracked.

In order to model compressibility effects in the liquid slugs above and below the interaction zone in the coolant channel, an approximation to a correct compressible treatment was made. This consists of calculating an effective displacement of the slug at the interface with the interaction zone caused by the interaction zone pressure acting against the slug and compressing it. This phenomenon can have a significant effect on the interaction zone pressure for the case of ejection into an unvoided channel during the first 1-2 msec. A comparison was made with PLUTO1[13] which uses a rigorous compressible treatment for its liquid slugs. The preliminary conclusion is that the approximation used in EPIC somewhat overpredicts the compression of the slugs, although its inclusion gave much better agreement with PLUTO1.

Considerable time was spent comparing EPIC with PLUTO1 for a TOP test case. EPIC's velocities in the fuel pin cavity next to the failure node are about twice as high as PLUTO's during the first 5-10 msec of the transient and the mass of fuel ejected from the pin into the channel in EPIC is about 25% higher than that in PLUTO. Although EPIC's equilibrated pressure at the failure location is lower than PLUTO's during the first 0.5 msec, it is consistently higher until about 6 msec, after which there is fair agreement. The velocities of the liquid sodium slugs in the channel are 60-70% higher in EPIC than in PLUTO.

Almost all of the difference between EPIC and PLUTO1 in mass of fuel ejected and in the velocities of the fuel froth in the molten fuel cavity can be explained by the different numerical techniques used in the two codes for the hydrodynamics in the fuel pin. Although both techniques use Eulerian cells, PLUTO1 uses a full cell-centered calculation. EPIC uses a cell-edge velocity calculation with cell-centered pressures and densities.

Cell-centered schemes are numerically unstable and in PLUTO stability was achieved by the introduction of an artificial viscosity term. Since a cell-centered scheme uses a pressure gradient across cells N+1 and N-1 in order to calculate an acceleration at cell N, the effect of local high pressure gradients such as occur near a pin rupture is mitigated. Also mitigating the effect of sizeable pressure gradients near the rupture is the artificial viscosity term which can dominate the real physical effects. It was seen in the example case used to compare with EPIC that the artificial viscosity term became so large on occasion that it was larger than the pressure gradient term in the momentum equation, causing a negative change in velocity near the failure node when there was a positive pressure gradient of tens of atmospheres.

In order to eliminate such spurious effects, we adjusted the artificial viscosity term to zero in PLUTO1. This produced such instabilities that the calculation was no longer meaningful. Our next step was to adjust the magnitude of the artificial viscosity term to be no larger than a certain fraction of the pressure gradient term. When the artificial viscosity term was reduced as much as it could be without causing instabilities in

the calculation, PLUTO agreed much better with EPIC. There still was significant disagreement however. Therefore, it was thought that the only way to actually compare the two codes was to put a cell-edge velocity calculation into PLUTO so that its pin model would be substantially the same as EPIC's. When this was done, there was very close agreement in the mass of fuel ejected from the pin and in the fuel velocities inside the pin. In fact, after 10 msec., instead of EPIC's mass of fuel in the channel being 25% higher than PLUTO's the two masses were exactly the same, although they differed at points along the way by as much as 10-12%. The fuel velocities within the pin were also in agreement to within 10-15%.

We believe that the differences remaining between PLUTO and EPIC are caused by the different models in the coolant channel. After changing to a cell-edge velocity scheme in PLUTO, the liquid sodium slug velocities in PLUTO increased by 30%, explaining half the difference with EPIC. The pressures calculated by PLUTO at the failure node were much closer to EPIC's after this change was made but were still considerably lower on average over the first 6-8 msec.

PLUTO's liquid slugs are driven by a consistently lower pressure than in EPIC partly because of the way that the Lagrangian cells in the channel are cut to form new cells. During the first 2 msec, there is fairly good agreement between PLUTO and EPIC in both liquid slug velocities and the equilibrated pressure in front of the rupture in the channel, although EPIC seems to have somewhat lower pressures during the first msec because of the overcompensation inherent in the approximate compressible treatment. This pressure is what drives the slugs. From 2-6 msec, however, PLUTO's pressures are substantially lower in front of the rupture and quite a bit lower still between the node in front of the rupture and the liquid slug. The latter effect is caused by cutting the expanding Lagrangian cell in front of the rupture when it gets too large. At this point, not enough fuel and fission gas has moved into the extremities of the original cell to pressurize the ends to the same extent as the center is and consequently there is a substantial pressure drop from the cell in front of the rupture to the smaller cells adjacent to the middle cell, and the pressure of the smaller, less pressurized cells is what drives the slugs.

In EPIC, materials in the coolant channel are homogenized for the purposes of the pressure equilibration over the length that the particles have penetrated up to a maximum of one Eulerian cell away from the failure cell. Thus during the first 5-6 msec the liquid slug is not "insulated" from the effect of the rupture node pressure by smaller, less pressurized cells as in PLUTO. Therefore the liquid slugs in EPIC are driven by a significantly higher pressure than PLUTO.

The reader should bear in mind the several parameters in PLUTO1 were adjusted to fit experimental data and that adjustment will need to be redone for EPIC because of the numerical calculational differences.

2. Recriticality Studies (P. B. Abramson)

In order to be able to examine the influence of local surface pressure pulses on the behavior of boiling fuel/steel pools, it was found

that rather major development efforts in the hydrodynamic portions of pool were necessary. These modifications are necessitated by the fact that continuing local pressures in a compressible fluid cause the fluid to pile up on the boundaries of the pressurized region, forming incompressible regions. To adequately describe these motions, POOL was modified to use fully the Particle In Cell (PIC) technique of Evans and Harlow[14] as well as an incompressible flow algorithm corresponding to zero vorticity presented by Hirt, Nichols & Romero[15] and described in our previous quarterly report.

We have found that this technique is stable and appears to converge well for the material motions we wish to follow, but that the incompressible algorithm appears to cause the loss of kinetic energy from the fluid. We postulate that this is due to the application and propagation of zero outflow conditions at the boundary of the incompressible region in combination with our ignoring pressure (density) waves in the incompressible regions. The primary effects are two:

a. We are able to follow the aspects of local pressurization in what appears to be a realistic fashion much farther than the old POOL algorithms would permit and far enough that we hope to be able to examine the neutronic behavior for recriticality under such conditions. Figure 2.a. shows the particle distribution 3 milliseconds after applying a localized 10 atm over pressure in a ring at half the maximum radius (this distribution is indicative of the maximum displacement that we were realistically able to track in the motions with the old POOL algorithms because single phase regions have now become locally significant). Figure 2.b. shows the influence of the same pressurization after 10 milliseconds. The material has moved in the manner shown because of the particular way in which this local pressure was allowed to spread and indicates the degree of motion that may now be examined. It is important to recognize that the neutronic response to such local pressurization is singularly determined by how and what pressure is applied and that no mechanistic way exists for determining such pressurizations.

b. The influence of the PIC treatment combined with our incompressible algorithms is to significantly reduce the fluid kinetic energy in single phase regions. This means that we may underestimate velocities and hence ramps. Since we have no vapor/liquid slip, this could be a compensating aspect on liquid motions; however, it may incorrectly change fluid kinetic energy and hinder the use of this algorithm in assessing the importance of heat transfer on work energy through examination of fluid kinetic energy.

More work needs to be done in this area before a numerical technique is settled on, and it may be that each class of problems needs its own particular one.

3. Importance of Heat Transfer in Disassembly Work Energy Estimates (P. B. Abramson)

We have found that the fluid kinetic energy may not be the most illustrative parameter to use in estimating the importance of fuel to steel heat transfer in assessing work energy. Thus, we are currently in the

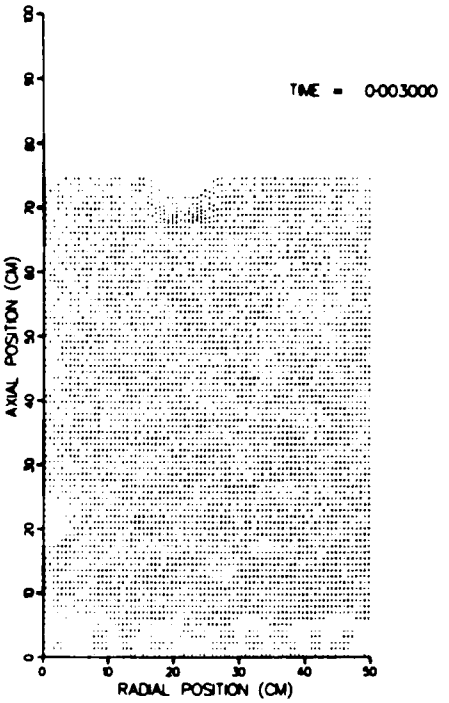

Fig. 2.a. Response to Local Pulse.

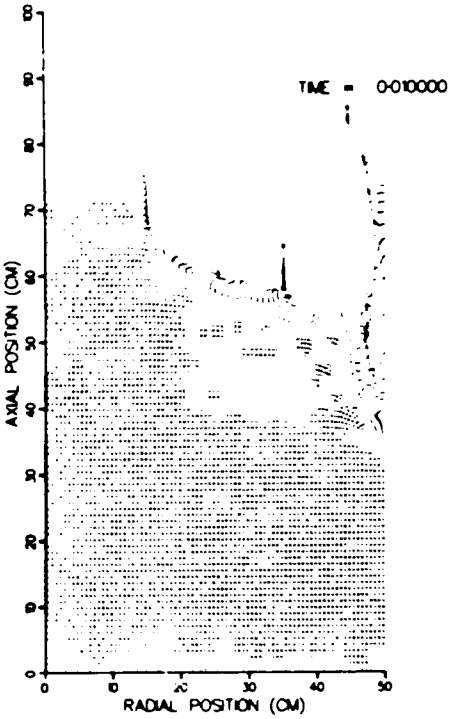

Fig. 2.b. Response to Local Pulse.

process of incorporating a thermodynamic potential energy model identical to the one in use in VENUS, so that we can demonstrate variation in an already accepted descriptor of accidents. To date we have examined the importance of fuel/steel heat transfer out to 30 ms following a hypothetical $50/second HCDA in a 1000 MWe plant. For that scenario, heat transfer from fuel to steel can serve to reduce the fluid kinetic energy by up to a factor of five. For a zero heat transfer case, the fluid kinetic energy continues to grow while, for even very small fuel to steel heat transfer, we have found that fluid kinetic energy decreases within a few milliseconds after the prompt burst. This appears to be due to both the incompressible regions and to the sink of pressure source into the cold steel.

IV. COORDINATION OF RSR SAFETY RESEARCH

A copy of the KACHINA code was received from LASL. It will be converted to the IBM 370 for possible incorporation into FX2-POOL.

Copies of FX2POOL and FX2POOLVENS were given to BNL. D. Majumdar was informed on the uses of this code. It was suggested to him that development of a more sophisticated (and realistic) treatment of the boundary heat transfer would be a worthwhile activity for BNL which would enhance the usefulness of FX2-POOL.

The DEMO 3 code was received from BNL and will be converted to the IBM 370.

P. Abramson attended an ACRS subcommittee meeting on SAREF on March 3rd and a meeting with DPM personnel and consultants on transition phase and SAS-FCI on March 19th.

P. Abramson and H. Hummel attended a meeting on GCFR safety at ANL on March 9th.

R. Curtis of NRC was assisted in defining the format and schedule for a meeting of RSR principal investigators to be held in April. This meeting is to be a starting point for coordination of RSR code validation work.

V. EVALUATION OF PROGRESS IN SAFETY RESEARCH

A. Effect of Neutron Streaming in Analysis of Critical Experiment Sodium Void Effect Measurements (H. H. Hummel)

A rather impressive improvement in consistency of C/E ratios for sodium voiding experiments in ZPPR Assembly 5 has been found[16-19] by using directional diffusion coefficients calculated by Benoist's theory.[10] C/E values with the corrections are still above unity, and are generally around 1.2. The increase in the leakage component caused by streaming is quite large, amounting to 40 to 50%. The question naturally arises as to why this large an effect has not been more evident in the past. There have

been pin-plate comparisons which tended to be in rather clear agreement, suggesting that heterogeneity effects of any kind were not large. A review of these measurements reveals the following:

(1) There actually may have been a fair amount of streaming in the pin cells, which are on a square lattice and therefore have planar voids. Also, the pins are rather large (3/8 in. diameter) with a 1/4 in. space in between. Benoist multipliers have not yet been calculated for these cells. However, measurements in ZPPR-5 suggest that a correction to the leakage component of 30% might be in order, which would minimize observed pin-plate differences.

(2) Most of the comparisons have been done in ZPPR-2 in central zones of height ± 30.1 cm, for which the leakage component is only 25 to 30% of the spectral and capture components, which would minimize streaming effects. Limited off-center experiments were done in ZPPR-2, but they have not been analyzed.

(3) The pin-plate comparisons in ZPPR-5 do indicate the presence of streaming, but have not yet been analyzed from this point of view.

Off-center measurements have been made in ZPPR-3, but their analysis has not been carried to the point when any conclusions can be drawn relative to streaming. C/E values for the corrected calculations for ZPPR-3 (done with ENDF/B-IV), mostly around 1.2, are consistent with the central worth discrepancy of fuel. This suggests that this discrepancy may be in the conversion from inhours to %k, although evaluations of delayed neutron data have not provided justification for this hypothesis. Experimental results for sodium void worth from the FTR-EMC[20] are also consistent with the hypothesis that all experimental results should be multiplied by a factor of about 1.2 in converting from inhours to %k, and that a streaming correction of 1.4 to 1.5 should be applied to the calculated leakage component of the sodium void effect to match experimental results. In analysis of the measurements reported in HEDL-TME-74-31,[20] the central C/E is 1.23, but in the outer part of the core, when the leakage component is practically the whole effect, C/E = 0.83. However, if it is assumed that C/E should be 1.23 throughout, this would be consistent with a streaming multiplier of 1.48 for the leakage component.

The most reasonable assumption for accident calculations seems to be not to make the bias adjustment to the calculations made in HEDL-TME-74-31, but to assume that the calculated values are correct, and that the discrepancy with experiment is due to a combination of ih/%k conversion error and to a large streaming correction.

B. Assessment of Potential for Recriticality (P. B. Abramson)

There are currently three general areas of effort being made to assess the potential for an energetic recriticality. These are:

1. Simple Phenomenologic Analyses
2. Complex Computer Analyses
3. Simulation Experiments

Each of these areas has its specific accomplishments and contributions as well as its faults. None has been able to prove that an energetic recriticality is impossible, but neither has any suggested a specific mechanism which might cause such an event. While there appears to be a "gut" level feeling among most investigators that the potential energetics are small, few investigators are willing to state that highly energetic events are impossible.

A meeting was convened at Argonne National Laboratory on April 5 and 6 at the request of W. H. Hannum (ERDA) to discuss the state of knowledge regarding energetic recriticalities. Most of the following information was presented at that meeting.

1. Accident Scenarios Leading to Recriticalities

A potential for secondary criticality was discussed for two very different times in the accident scenario.

First, there is the potential for autocatalytic events such as an LOF-driven TOP or recompaction from fuel motion. The potential currently exists or will exist in the near future (1 year or so) to mechanistically examine such energetics in a manner similar to the SAS analysis of accident initiation. Events that might take place when geometry is intact or nearly so are much more amenable to deterministic (mechanistic) analysis than those which occur late in the accident sequence.

Second, and perhaps the more significant issue in the meeting was the potential for recriticality in a grossly disrupted geometry. Because of the largely unknown state of the system after accident initiation, this area of study is open to speculation. Many investigators have pointed out the difficulty of mechanistic analysis when the state of the system is largely unknown. Furthermore, some investigators, including those who prepared the CRBR PSAR, have felt it to be more effective to fall back from mechanistic analysis to simple phenomenology in the search for understanding. It is this second area where we shall concentrate this report.

2. Phenomenology of Molten Fuel/Steel Pools

A significant effort has been mounted in the Reactor Analysis and Safety Division to attempt to demonstrate that boiling fuel/steel mixtures are monotonically dispersive, self-regulating, and in general not susceptable to recompaction. However, there are other efforts (specifically at UCLA) which purport to refute some of the "evidence" gathered by the former.

An investigation by Fauske, et al.,[21] at ANL has applied some basic two-phase flow stability criteria to one-dimensional internal heat generating pools to conclude that even for very low power levels, the fuel/steel mixture will be in the churn turbulent flow regime and will have roughly 50% void fraction due to the upward flux of steel vapor.

These same investigators have presented arguments based upon both simple membrane stability theory and basic thermodynamics that a boiling fuel/steel pool enclosed by a melting steel container will be encased in a stable thin fuel crust, which acts as a limiting mechanism for boundary heat transfer out of the pool.

Another investigation by Abramson[22] at ANL was a simple thermodynamic analysis to develop basic regimes of stable behavior of such pools in terms of ratios of fuel mass to steel mass and fuel and steel temperature, based upon the total local vapor pressure as a dispersive source term.

V. Dhir and I. Catton and their co-workers at UCLA have performed basic thermodynamic, hydrodynamic analyses and experiments which establish criteria for the formation of a water or benzene crust at the bottom of a liquid pool whose lower boundary is vapor generating CO_2. They feel that these criteria may be extended to a fuel/steel system for which the major difference is that the solid (steel or CO_2) is separated from the liquid (UO_2 or H_2O) by a liquid (steel) instead of a vapor (CO_2) layer. While this extension remains to be either experimentally or analytically demonstrated, the UCLA investigators have modified an analysis of film boiling heat transfer by Berenson[23] and report that an extension to the film melting of steel at its melting temperature, by UO_2 at its melting temperature would give a very large downward heat flux by the melting attack (on the order of 20-30% of full power). Furthermore, the influence of the mixing caused by rising bubbles in the UCLA experiments described above has been so large that the pool temperature profile remains nearly uniform until crust formation begins. This has been interpreted by them as suggesting that even internal heat generation may not cause internal boiling at low power because of the good mixing.

The major issue regarding the behavior of a fuel/steel pool is whether it remains dilute or can become fully dense. Fauske has maintained that internal heating causes enough internal vapor generation to cause the pool to be in a churn turbulent flow (dilute) regime and that a stable fuel crust on the boundaries of the pool regulates the boundary heat fluxes. Dhir and Catton have suggested that a fuel crust may not form and that, if it does not, the melting attack on the steel below could absorb significantly more power than is generated at decay heat. Furthermore, Dhir and Catton have suggested that the rising of steel droplets through a fully dense liquid fuel pool will create enough mixing to suppress internal boiling and cause all energy generated internally to be removed at the boundaries, thus causing such a pool to remain in a bubbly flow (dense) state.

This debate therefore suggests two families of experiments and some analysis: one set of experiments to determine the ability of rising drops/bubbles coupled with large downward heat transfer to suppress internal nucleation at low power microwave heating, and a second series of experiments, coupled to analysis, to determine the validity of extending the Berenson analysis of a liquid/vapor/solid system to a liquid/liquid/solid system for heat transfer. In particular, this should include experiments with liquid/liquid/solid systems to determine crust formation and stability criteria as has been done for the liquid/vapor/solid system at UCLA.

3. Experimental Simulation of Boiling Fuel/Steel Pools

To date, the experimental effort has concentrated on three general phenomena.

a. The boiling of water by microwave heating,
b. The boiling of salt water by direct current heating,
c. Some recent attempts to examine simulant crust formation.

In both the cases of salt water direct electrical heating and of the microwave heating of pure water the experiments have concentrated upon correlations for radial and axial boundary heat fluxes. All these experiments give good indication that the flow is churn turbulent and very disruptive.

Recent experiments have been conducted at ANL which indicate the stable formation of a crust between freon and water, while recent experiments at UCLA indicate that criteria can be established which define the system state necessary to permit crust formation between solid CO_2 and water and between solid CO_2 and benzene. Both experiments were attempts to test the validity of the hypothesized crust formation between fuel and steel at the boundaries of a boiling pool. Each investigator is convinced that his experiments accurately test that hypothesis.

There have been no experiments which were directed at determining the behavior of boiling pools of two materials, nor have there been any efforts to determine internal energy fluxes or pressure profiles.

4. Computer Modeling Efforts

a. TRANSIT - is the first attempt to determine how an accident might lead to a molten core pool. It models the thermodynamic behavior of a melting core, following subassembly to subassembly propogation of melting, but does no hydrodynamic modeling.

b. FX2-POOL - treats the motions of homogenized fuel steel mixtures in R-Z geometry assuming no slip, and parametrically treats heat transfer between fuel and steel both in the pool and at the boundaries. This is basically a parametric scoping tool.

c. SIMMER - treats the motions of two materials with liquid, vapor and solid of each material interpenetrating with slip. Furthermore, the SIMMER models treat the interphase and intermaterial momentum, mass and energy transfer mechanistically.

This is the ultimate code - when the basic material distribution functions and properties are known, SIMMER should be able (at fairly large cost) to deterministically follow nearly any motions. The basic problem will be the gathering of proper input data.

d. FX2-VENUS III - has capabilities between FX2-POOL and SIMMER.

5. Regions of Needed Research

a. Determination experimentally and development of analytical tools to follow accident initiation farther than SAS. (The transition to a boiling pool - perhaps by adaptation of TRANSIT and SIMMER)

b. Experiments to determine basic fuel/steel thermohydraulic behavior including:

   i. basic material size and distribution functions
   ii. pool hydrodynamic behavior
   iii. crust formation and stability studies with systems that simulate the fuel/steel situation
   iv. potential modes of recompaction.

c. In-pile experiments with real materials.

6. Summary

There appears to be a growing opinion that above and below core plugging is very likely, and will cause a boiling pool of fuel and steel. Many investigators are of the opinion that incoherencies make the likelihood of formation of a whole core pool small. Phenomenologic modelers have conflicting views regarding boiling fuel/steel pool behavior. The computer analysts have adequate models under development, but seriously lack useful basic experimental data. Most investigators feel there is a low probability for significant energetics after initiation, but few feel the probability is zero, and there is currently no mechanistic method for bounding these low probability high energetics phenomena.

MONTE CARLO ANALYSIS AND CRITICALS PROGRAM PLANNING FOR SAFETY-RELATED CRITICALS (A2018)

VI. MONTE CARLO ANALYSIS OF SAFETY-RELATED CRITICALS (E. M. Gelbard)

Monte Carlo calculations in support of the preanalysis of future DEMO safety-related criticals have yielded the following results for R-Z model eigenvalue calculations:

	Diffusion Theory	Monte Carlo
Reference Core	1.0	0.998 ± 0.002 (60 K Histories)
Final Phase Damaged Core	1.0	1.013 ± 0.003 (100 K Histories)

There is good agreement between the Monte Carlo and diffusion calculations for the reference (undamaged) core. The 1% eigenvalue difference in the results for the damage core is statistically significant and has prompted further R-Z model studies using diffusion, transport and Monte Carlo calculations.

It is expected that TWOTRAN will play an important role in the analysis of the final phase damaged core. In order to gain experience with TWOTRAN it was decided that TWOTRAN should be used, initially, to calculate the reference core. The TWOTRAN eigenvalue turned out to be higher than the diffusion theory and Monte Carlo eigenvalues by about 1%. Cross sections in TWOTRAN have been carefully checked, and seem to be identical with those used in the diffusion calculation. The discrepancy is still under investigation.

VII. PLANNING OF DEMO SAFETY RELATED EXPERIMENTS

The previous quarterly report discussed the results of core design scoping calculations for a number of alternate reactor compositions. One design was selected for use as the reference design for additional program planning. This reference design is based on Composition No. 3 with an H/D ratio of 1.0. A number of basic physics parameters, including fissile loadings, central-core real and adjoint spectra, and central-core reaction rates and ratios, have previously been reported for this design. Additional calculated results for this reference design are presented at this time. The material inventory requirements for the reference program are also reviewed.

A. Analysis for Reference Design

Central and axial traverse material worths and Doppler reactivity effects have been calculated for two possible configurations in a meltdown sequence for this core. These configurations, Step 1 and Step 5, correspond to the reference and 37-drawer slump-zone configurations as shown in Fig. 3. The reactivity worths at core center for ^{235}U, ^{238}U, ^{239}Pu, ^{240}Pu, sodium, and iron are listed in Table III. The central reactivity worths of these materials in the Step 5 configuration increase (as compared to the Reference Step 1) due to the smaller core volume and fissile mass (381.97 liters and 227.79 kg as compared to 618.64 liters and 368.93 kg) and to the higher density of fissile material at the core center. Also listed in Table I are the ratios of these central worths in the two configurations. The significant variation in this ratio indicates the strong spectral shifts which occur between the two cores. The fission-source component of the worths of the threshold elements, ^{238}U and ^{240}Pu, are increased in the much harder spectrum of the Step 5 configuration. These shifts in the real and adjoint spectra are shown in Table IV.

The reactivity worths of these materials as a function of axial position are listed in Tables V-X and are shown graphically in Figs. 4-9. The differences in the worth profiles can be physically interpreted as follows. The positive fission production and negative absorption and downscattering

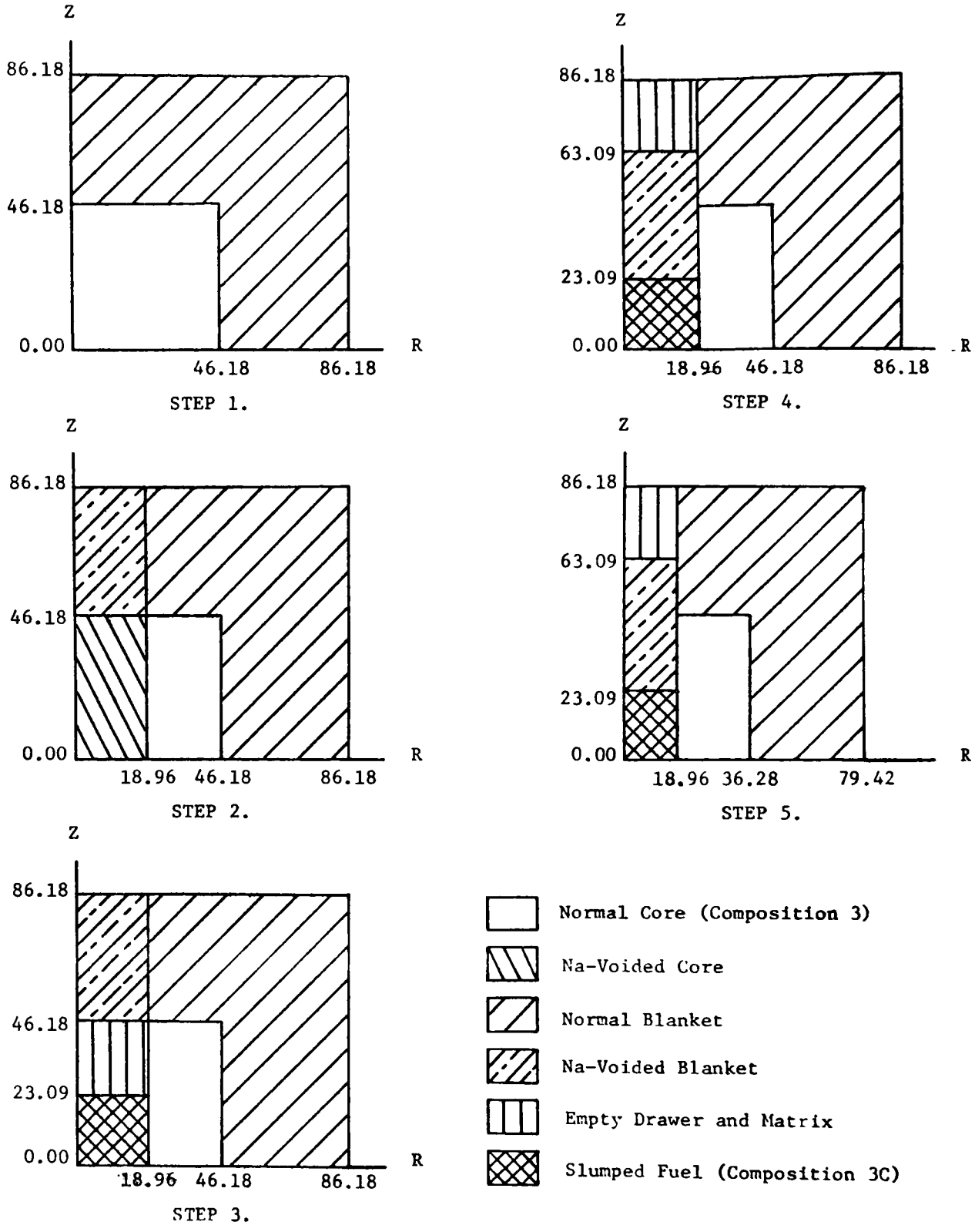

Fig. 3. Two-Dimensional (R-Z) Models for HCDA Sequence 37 Drawer Slump Zone. ANL Neg. No. 116-76-81.

TABLE III. Central Material Worths for the Step 1 (Reference) and the Step 5 (Slumped Fuel) Configurations

	Step 1	Step 5	Step 5 / Step 1
Prompt Neutron Lifetime, sec	3.276358^{-7}	2.119566^{-7}	
β_{eff}	3.134335^{-3}	3.293866^{-3}	
Reactivity Conversion Factor, Ih/%ρ	979.0896	958.5312	
Material Worths, Ih/kg			
^{235}U	342.42	757.98	2.2136
^{238}U	-22.506	-34.446	1.5305
^{239}Pu	470.03	1130.3	2.4047
^{240}Pu	80.086	286.60	3.5787
Na	-20.959	-56.430	2.6924
Fe	-12.233	-34.045	2.7830

TABLE IV. Comparison of Real and Adjoint Spectra at Core Center for the Step 1 (Reference) and the Step 5 (Slumped Fuel) Configurations

	Normalized Broad Group Real Fluxes, ϕ_i			Normalized Broad Group Adjoint Fluxes, ϕ_i^*		
Group, i	Step 1 Reference Configuration	Step 5 Slumped Configuration	$\frac{\phi_i(\text{Step 5})}{\phi_i(\text{Step 1})}$	Step 1 Reference Configuration	Step 5 Slumped Configuration	$\frac{\phi_i^*(\text{Step 5})}{\phi_i^*(\text{Step 1})}$
1	$3.2752E^{-3}$	$4.4860E^{-3}$	1.3697	$7.2132E^{-2}$	$7.4131E^{-2}$	1.0277
2	$1.3556E^{-2}$	$1.8225E^{-2}$	1.3444	$6.5362E^{-2}$	$6.4486E^{-2}$	0.9866
3	$3.4363E^{-2}$	$4.4961E^{-2}$	1.3084	$6.6238E^{-2}$	$6.5238E^{-2}$	0.9849
4	$5.2546E^{-2}$	$6.1811E^{-2}$	1.1763	$6.2842E^{-2}$	$6.1347E^{-2}$	0.9762
5	$6.8241E^{-2}$	$8.0940E^{-2}$	1.1861	$5.8460E^{-2}$	$5.6163E^{-2}$	0.9607
6	$1.1651E^{-1}$	$1.4611E^{-1}$	1.2541	$5.7481E^{-2}$	$5.4568E^{-2}$	0.9493
7	$1.0899E^{-1}$	$1.1072E^{-1}$	1.0159	$5.7087E^{-2}$	$5.5645E^{-2}$	0.9747
8	$1.2078E^{-1}$	$1.2686E^{-1}$	1.0504	$5.5787E^{-2}$	$5.4276E^{-2}$	0.9729
9	$1.2018E^{-1}$	$1.1615E^{-1}$	0.9664	$5.4826E^{-2}$	$5.3659E^{-2}$	0.9787
10	$9.5125E^{-2}$	$8.8176E^{-2}$	0.9269	$5.3595E^{-2}$	$5.2563E^{-2}$	0.9808
11	$7.4869E^{-2}$	$6.8340E^{-2}$	0.9128	$5.1722E^{-2}$	$5.0382E^{-2}$	0.9741
12	$5.2606E^{-2}$	$4.2973E^{-2}$	0.8169	$5.0344E^{-2}$	$4.8549E^{-2}$	0.9643
13	$5.3339E^{-2}$	$4.0591E^{-2}$	0.7610	$4.9551E^{-2}$	$4.6930E^{-2}$	0.9471
14	$3.4432E^{-2}$	$2.3166E^{-2}$	0.6728	$5.0679E^{-2}$	$4.8079E^{-2}$	0.9487
15	$1.6919E^{-2}$	$1.0630E^{-2}$	0.6283	$5.2100E^{-2}$	$4.9622E^{-2}$	0.9524
16	$1.0917E^{-2}$	$8.2596E^{-3}$	0.7566	$5.3244E^{-2}$	$5.0669E^{-2}$	0.9516
17	$3.8238E^{-3}$	$4.0688E^{-3}$	1.0641	$5.4540E^{-2}$	$5.3101E^{-2}$	0.9736
18	$1.0040E^{-2}$	$2.2157E^{-3}$	0.2207	$5.5647E^{-2}$	$5.4851E^{-2}$	0.9857
19	$5.4998E^{-3}$	$8.5382E^{-4}$	0.1552	$5.7133E^{-2}$	$5.6871E^{-2}$	0.9954
20	$2.6289E^{-3}$	$3.2844E^{-4}$	0.1249	$6.4920E^{-2}$	$6.4089E^{-2}$	0.9872
21	$9.2397E^{-4}$	$9.7981E^{-5}$	0.1060	$6.7110E^{-2}$	$6.7628E^{-2}$	1.0077
22	$4.1619E^{-4}$	$2.9938E^{-5}$	0.0719	$7.2859E^{-2}$	$7.3421E^{-2}$	1.0077
23	$1.4798E^{-5}$	$6.8668E^{-7}$	0.0464	$1.0465E^{-1}$	$1.0133E^{-1}$	0.9683
24	$2.6126E^{-7}$	$8.4396E^{-8}$	0.3230	$4.1944E^{-2}$	$5.5216E^{-2}$	1.3164
25	$1.1992E^{-8}$	$1.1278E^{-8}$	0.9404	$8.2317E^{-2}$	$8.0731E^{-2}$	0.9807
26	$1.3983E^{-8}$	$1.4968E^{-8}$	1.0705	$9.2829E^{-2}$	$9.7875E^{-2}$	1.0544
27	$6.9520E^{-9}$	$5.1624E^{-9}$	0.7426			

TABLE V. ^{235}U Axial Reactivity Worth Traverse, Ih/kg

HEIGHT ABOVE MIDPLANE	STEP 1. (REFERENCE)	STEP 5. (SLUMPED)
0.8880	342.4199	757.9824
2.6640	341.0527	748.9319
4.4400	338.3308	731.0273
6.2160	334.2793	704.6741
7.9920	328.9360	670.4492
9.7680	322.3506	629.1384
11.5440	314.5613	581.7246
13.3200	305.6555	529.3740
15.0960	295.6960	473.4258
16.8720	284.7834	415.4263
18.6480	273.0178	357.0586
20.4240	260.4871	300.2014
22.2000	247.3041	241.4899
24.3707	230.6090	189.4588
26.9361	210.0379	154.1409
29.5015	189.0655	127.3210
32.0669	168.1056	104.9195
34.6323	147.5722	86.0387
37.1977	127.8792	70.0720
39.7631	109.4693	56.5650
42.3285	92.7942	45.1641
44.8939	78.4171	35.8410
47.5859	66.7242	28.1732
50.4045	55.4214	21.2828
53.2231	45.2237	15.2127
56.0417	36.2063	10.3827
58.8603	28.3981	6.6408
61.6789	21.7752	3.8818
64.0502	17.0815	2.7134
65.9742	13.8064	2.4634
67.8982	10.9770	2.2320
69.8222	8.5586	2.0179
71.7462	6.5140	1.8210
73.6702	4.8085	1.6428
75.5942	3.4099	1.4850
77.5182	2.2899	1.3498
79.4422	1.4239	1.2391
81.3662	0.7921	1.1544
83.2902	0.3794	1.0973
85.2142	0.1755	1.0685

TABLE VI. ^{238}U Axial Reactivity Worth Traverse, Ih/kg

HEIGHT ABOVE MIDPLANE	STEP 1. (REFERENCE)	STEP 5. (SLUMPED)
0.8880	-22.5062	-34.4463
2.6640	-22.3935	-33.7624
4.4400	-22.1669	-32.4032
6.2160	-21.8313	-30.3892
7.9920	-21.3879	-27.7520
9.7680	-20.8405	-24.5304
11.5440	-20.1939	-20.7728
13.3200	-19.4546	-16.5387
15.0960	-18.6297	-11.8968
16.8720	-17.7243	-6.9271
18.6480	-16.7484	-1.7213
20.4240	-15.7093	3.6171
22.2000	-14.6169	3.4250
24.3707	-13.2310	-2.2416
26.9361	-11.5268	-4.8218
29.5015	-9.7911	-4.2922
32.0669	-8.0568	-3.6499
34.6323	-6.3570	-2.9995
37.1977	-4.7244	-2.3941
39.7631	-3.1892	-1.8575
42.3285	-1.7771	-1.3974
44.8939	-0.5064	-0.7462
47.5859	0.0545	0.2624
50.4045	0.0239	0.8718
53.2231	0.0425	0.8721
56.0417	0.0738	0.8799
58.8603	0.1024	0.8951
61.6789	0.1238	0.9168
64.0502	0.1283	0.9334
65.9742	0.1357	0.9546
67.8982	0.1407	0.9770
69.8222	0.1438	0.9977
71.7462	0.1456	1.0150
73.6702	0.1464	1.0283
75.5942	0.1467	1.0376
77.5182	0.1467	1.0436
79.4422	0.1464	1.0471
81.3662	0.1462	1.0488
83.2902	0.1459	1.0496
85.2142	0.1458	1.0498

TABLE VII. ^{239}Pu Axial Reactivity Worth Traverses, Ih/kg

HEIGHT ABOVE MIDPLANE	STEP 1. (REFERENCE)	STEP 5. (SLUMPED)
0.8880	470.0283	1130.2727
2.6640	468.1414	1116.3875
4.4400	464.3672	1088.9185
6.2160	458.7434	1048.4209
7.9920	451.3191	995.7776
9.7680	442.1677	932.1216
11.5440	431.3516	858.8911
13.3200	418.9690	777.7761
15.0960	405.1189	690.7813
16.8720	389.9246	600.1758
18.6480	373.5215	508.4839
20.4240	356.0454	418.5183
22.2000	337.6321	327.8528
24.3707	314.2852	249.1164
26.9361	285.4258	197.1971
29.5015	255.9128	158.3782
32.0669	226.3009	127.2266
34.6323	197.1330	101.9697
37.1977	168.9518	81.3323
39.7631	142.3368	64.4090
42.3285	117.8457	50.5163
44.8939	96.1134	39.3875
47.5859	77.6482	30.5141
50.4045	61.8137	22.6368
53.2231	48.6493	15.9260
56.0417	37.7752	10.6942
58.8603	28.8743	6.7179
61.6789	21.6669	3.8413
64.0502	16.7459	2.6481
65.9742	13.3889	2.4002
67.8982	10.5451	2.1720
69.8222	8.1548	1.9618
71.7462	6.1636	1.7696
73.6702	4.5236	1.5962
75.5942	3.1933	1.4432
77.5182	2.1376	1.3125
79.4422	1.3274	1.2055
81.3662	0.7396	1.1240
83.2902	0.3573	1.0690
85.2142	0.1689	1.0413

TABLE VIII. ^{240}Pu Axial Reactivity Worth Traverse, Ih/kg

HEIGHT ABOVE MIDPLANE	STEP 1. (REFERENCE)	STEP 5. (SLUMPED)
0.8880	80.0864	286.6023
2.6640	79.7769	283.1394
4.4400	79.1604	276.2739
6.2160	78.2417	266.1257
7.9920	77.0283	252.9114
9.7680	75.5275	236.8715
11.5440	73.7540	218.3426
13.3200	71.7178	197.7095
15.0960	69.4359	175.4412
16.8720	66.9243	152.0667
18.6480	64.2027	128.2352
20.4240	61.2908	104.6755
22.2000	58.2094	76.8618
24.3707	54.2805	48.8725
26.9361	49.3716	32.8409
29.5015	44.2883	23.6559
32.0669	39.1055	17.2147
34.6323	33.8981	12.6227
37.1977	28.7436	9.2998
39.7631	23.7192	6.8642
42.3285	18.9123	5.0614
44.8939	14.4430	3.9778
47.5859	10.1174	3.5694
50.4045	6.9150	3.1017
53.2231	4.7834	2.3212
56.0417	3.3443	1.7607
58.8603	2.3583	1.3706
61.6789	1.6734	1.1166
64.0502	1.2542	1.0265
65.9742	0.9950	1.0275
67.8982	0.7896	1.0316
69.8222	0.6267	1.0359
71.7462	0.4975	1.0386
73.6702	0.3957	1.0391
75.5942	0.3160	1.0375
77.5182	0.2546	1.0345
79.4422	0.2087	1.0307
81.3662	0.1760	1.0271
83.2902	0.1550	1.0243
85.2142	0.1447	1.0228

TABLE IX. Sodium Axial Reactivity Worth Traverse, Ih/kg

HEIGHT ABOVE MIDPLANE	STEP 1. (REFERENCE)	STEP 5. (SLUMPED)
0.8880	-20.9591	-56.4304
2.6640	-20.7719	-54.3638
4.4400	-20.4013	-50.2482
6.2160	-19.8486	-44.1163
7.9920	-19.1189	-36.0195
9.7680	-18.2187	-26.0243
11.5440	-17.1556	-14.2162
13.3200	-15.9386	-0.6995
15.0960	-14.5768	14.4020
16.8720	-13.0841	30.9472
18.6480	-11.4724	48.8144
20.4240	-9.7554	68.0025
22.2000	-7.9488	61.1913
24.3707	-5.6426	25.7154
26.9361	-2.8169	4.9407
29.5015	0.0655	1.4534
32.0669	2.9460	-0.2582
34.6323	5.7622	-0.9735
37.1977	8.4458	-1.1371
39.7631	10.9179	-1.0099
42.3285	13.0764	-0.7455
44.8939	14.7640	0.8245
47.5859	13.2149	4.3010
50.4045	9.6055	6.0910
53.2231	6.9014	5.3614
56.0417	4.9300	4.8661
58.8603	3.5254	4.5592
61.6789	2.5438	4.4013
64.0502	1.9352	4.3679
65.9742	1.5859	4.4282
67.8982	1.3201	4.4963
69.8222	1.1193	4.5599
71.7462	0.9685	4.6115
73.6702	0.8562	4.6483
75.5942	0.7733	4.6709
77.5182	0.7131	4.6819
79.4422	0.6703	4.6850
81.3662	0.6411	4.6836
83.2902	0.6231	4.6808
85.2142	0.6144	4.6788

TABLE X. Iron Axial Reactivity Worth Traverse, Ih/kg

HEIGHT ABOVE MIDPLANE	STEP 1. (REFERENCE)	STEP 5. (SLUMPED)
0.8880	-12.2331	-34.0451
2.6640	-12.1470	-33.1520
4.4400	-11.9755	-31.3731
6.2160	-11.7200	-28.7258
7.9920	-11.3832	-25.2325
9.7680	-10.9672	-20.9252
11.5440	-10.4757	-15.8406
13.3200	-9.9130	-10.0246
15.0960	-9.2832	-3.5334
16.8720	-8.5922	3.5611
18.6480	-7.8457	11.1596
20.4240	-7.0496	19.1178
22.2000	-6.2108	17.7503
24.3707	-5.1395	6.9323
26.9361	-3.8199	1.0347
29.5015	-2.4666	0.4305
32.0669	-1.1026	0.1394
34.6323	0.2482	0.0276
37.1977	1.5617	0.0132
39.7631	2.8113	0.0469
42.3285	3.9632	0.0997
44.8939	4.9590	0.5774
47.5859	4.7623	1.7545
50.4045	3.6147	2.3153
53.2231	2.7126	1.9974
56.0417	2.0200	1.7687
58.8603	1.4985	1.6142
61.6789	1.1126	1.5209
64.0502	0.8605	1.4925
65.9742	0.7083	1.5102
67.8982	0.5875	1.5306
69.8222	0.4923	1.5494
71.7462	0.4177	1.5642
73.6702	0.3599	1.5741
75.5942	0.3155	1.5794
77.5182	0.2821	1.5811
79.4422	0.2575	1.5803
81.3662	0.2403	1.5786
83.2902	0.2294	1.5767
85.2142	0.2242	1.5756

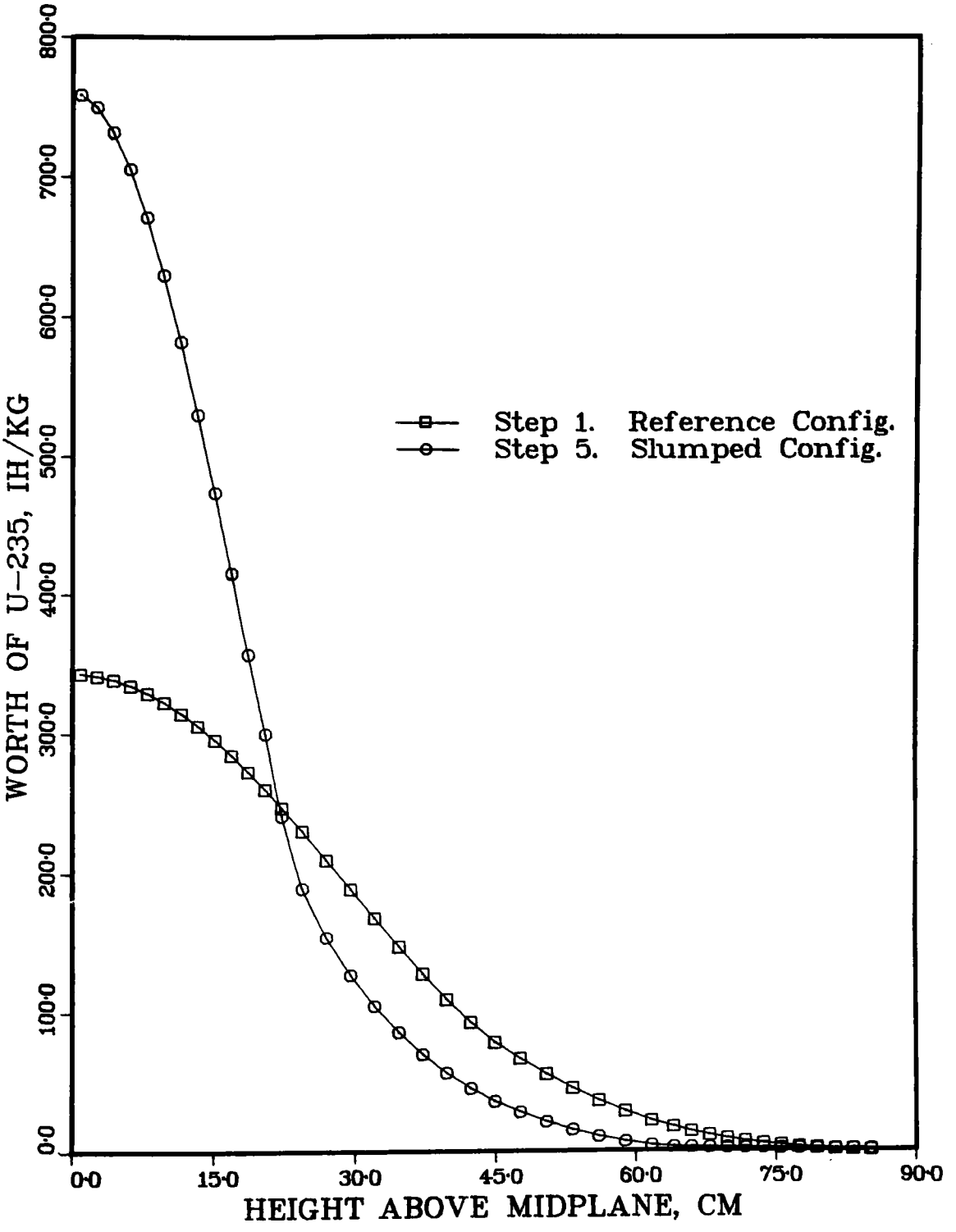

Fig. 4. ^{235}U Axial Reactivity Worth Traverse.
ANL Neg. No. 116-76-79.

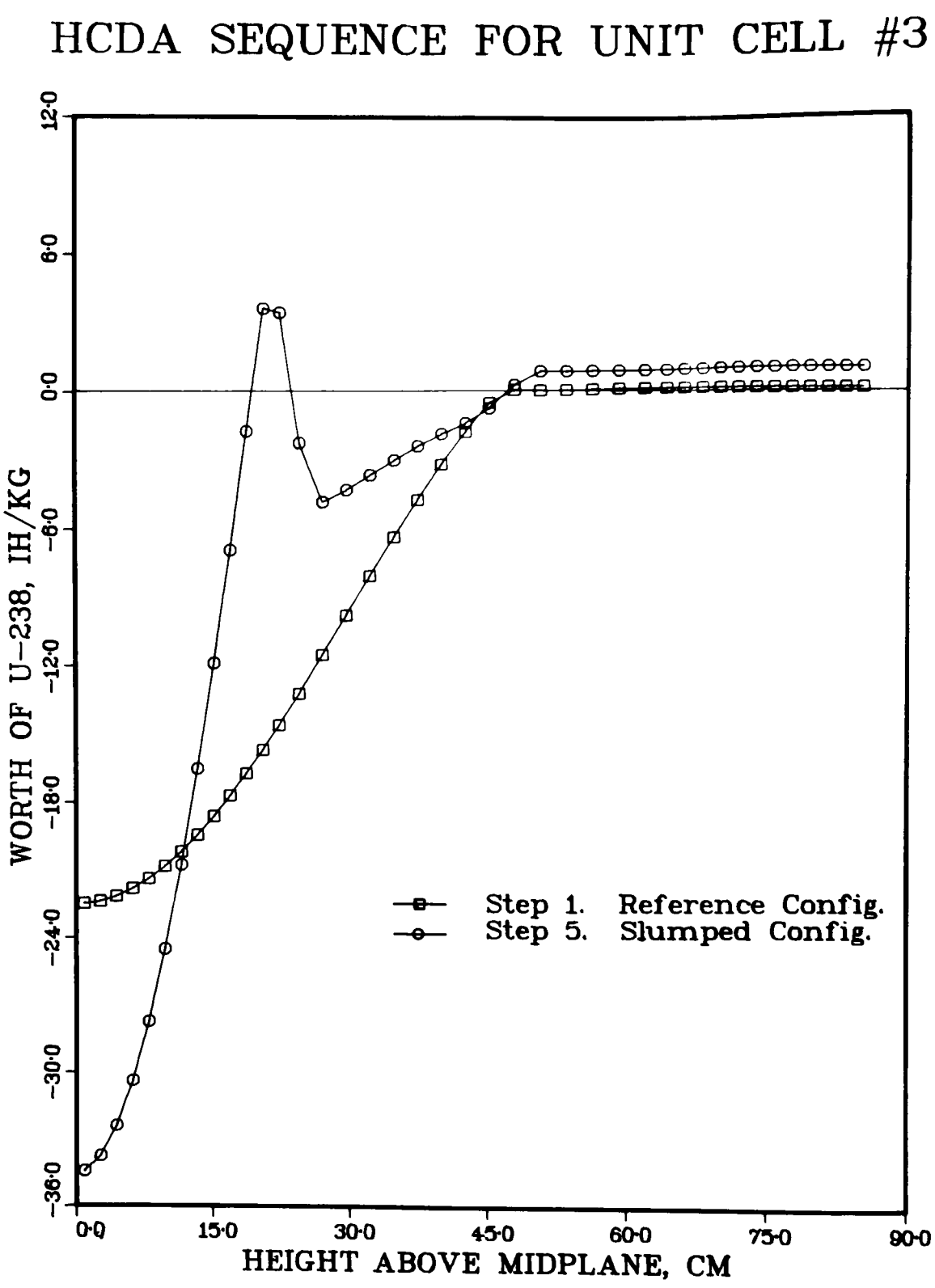

Fig. 5. ^{238}U Axial Reactivity Worth Traverse.
ANL Neg. No. 116-76-80.

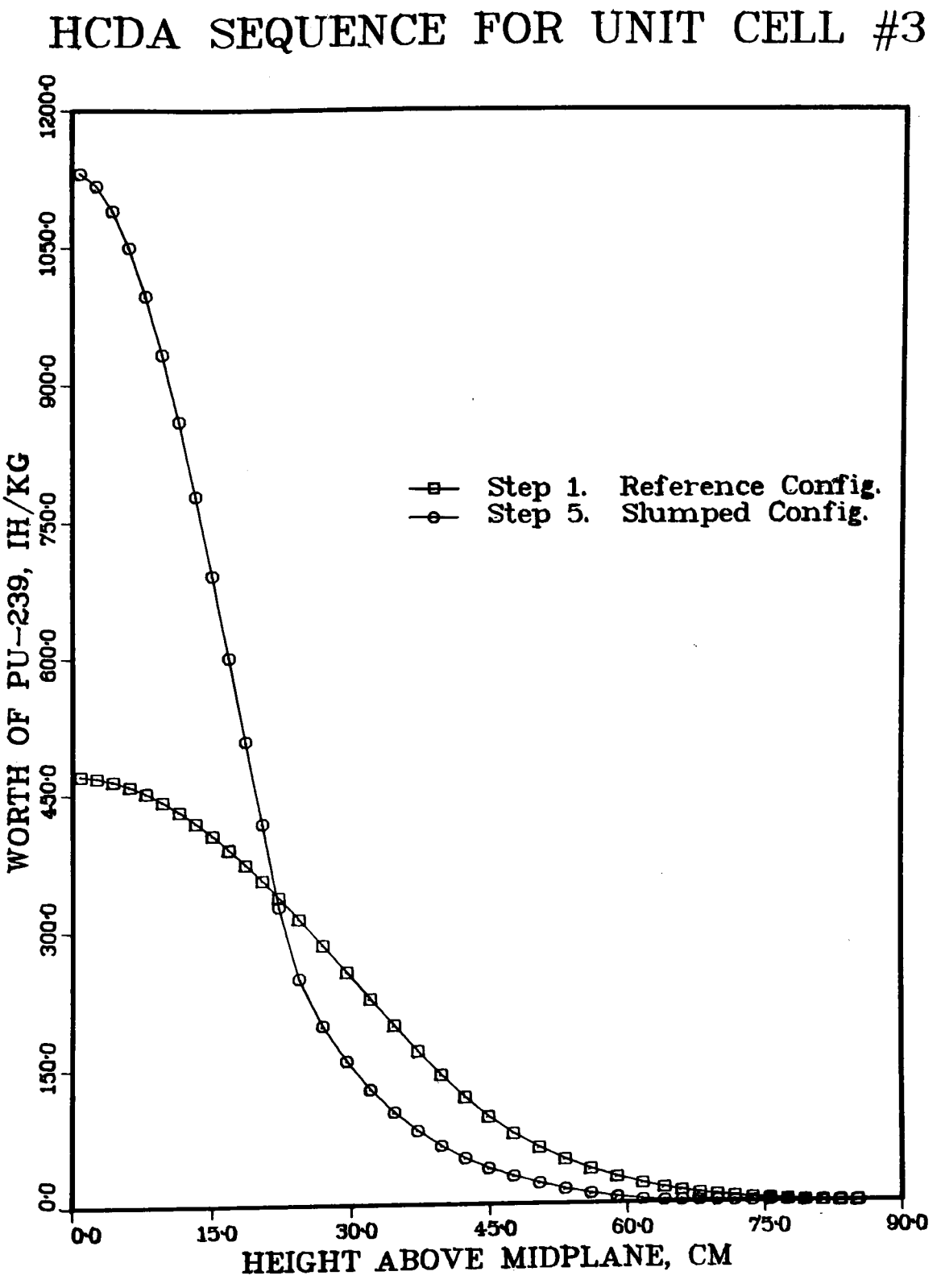

Fig. 6. ^{239}Pu Axial Reactivity Worth Traverse.
ANL Neg. No. 116-76-77.

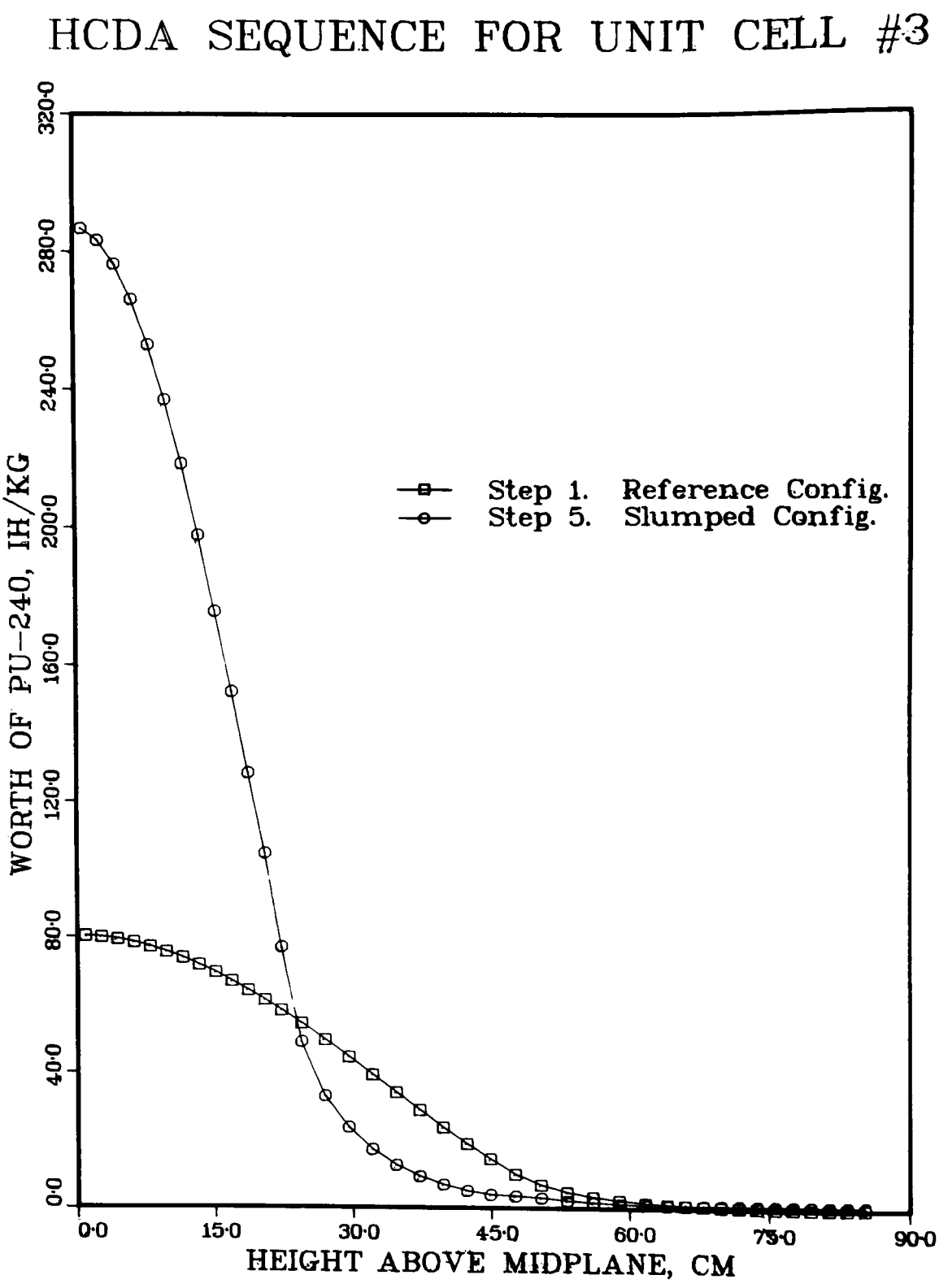

Fig. 7. ^{240}Pu Axial Reactivity Worth Traverse. ANL Neg. No. 116-76-85.

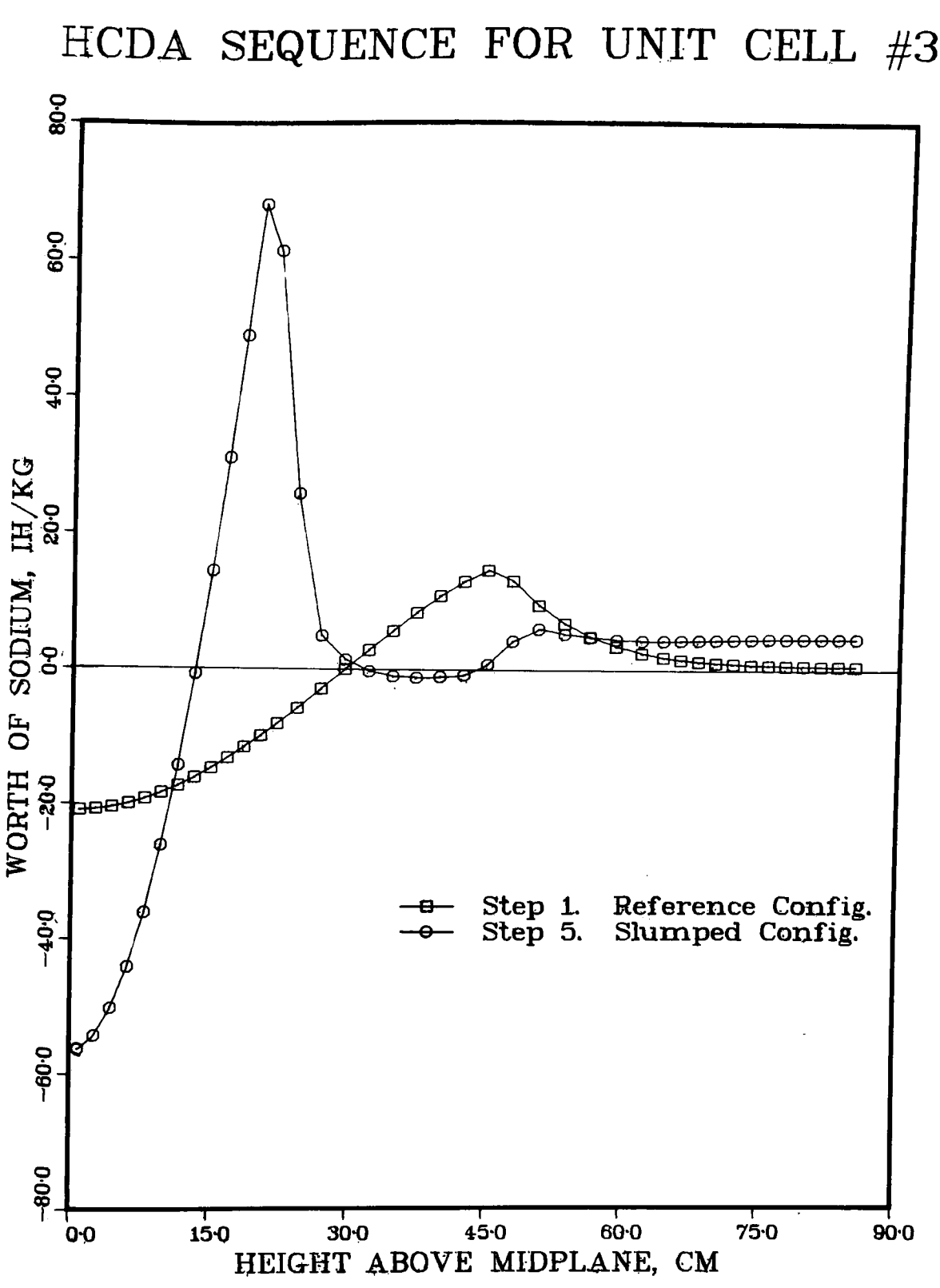

Fig. 8. Sodium Axial Reactivity Worth Traverse.
ANL Neg. No. 116-76-84.

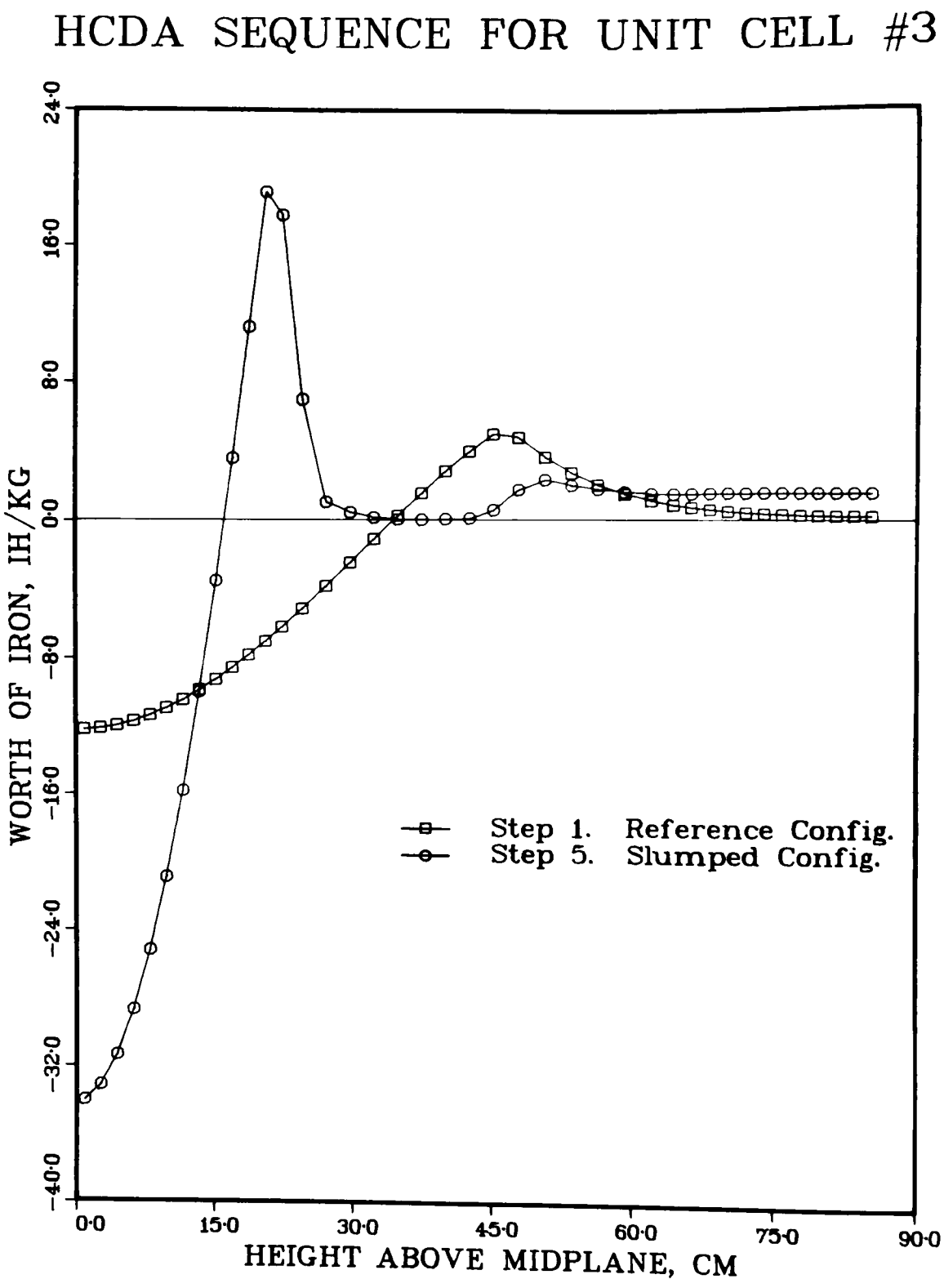

Fig. 9. Iron Axial Reactivity Worth Traverse.
ANL Neg. No. 116-76-83.

worth components of ^{235}U, ^{239}Pu, and ^{240}Pu follow the same trend as the flux profiles in the two configurations. The positive leakage component of ^{238}U increases due to the strong flux and adjoint gradients as the core/axial-blanket interface is approached. It should be noted the core/axial-blanket interface is 46.18 cm in Step 1 and 23.09 cm in Step 5. This positive effect of ^{238}U at the core boundary is the result of neutron reflection back toward the core. A similar effect is produced for the scattering materials, sodium and iron. Their small negative worth at the core center, which is the sum of capture and downscattering components, is overpowered by the leakage component at the core-blanket interface where these materials act as reflectors. The physical interpretation of the axial worth curves for positions deeper into the collapsed blanket and completely outside of this blanket require further examination.

Doppler reactivity effects have been calculated for these two configurations. The full core isothermal Doppler reactivity effect was calculated by eigenvalue difference upon replacing the cross sections from the base broad group set (T = 300°K) with cross sections from a high temperature broad group set (T = 3000°K) for all the heavy resonance absorber materials (^{239}Pu, ^{240}Pu, ^{241}Pu, ^{242}Pu, ^{241}Am, ^{235}U, and ^{238}U). The results are summarized in Table XI. The sharp decrease (-36% relative to the reference configuration) in the Doppler reactivity effect in the Step 5 configuration is predominantly due to the much harder spectrum. In both configurations the Doppler effect is primarily the ^{238}U component with a small net positive contribution from the remaining heavy elements.

B. Material Inventory Requirements for Reference Design

In general, this reference design uses the same materials that are available and are being used in the current ZPR/ZPPR programs. The mass requirements are listed in Table XII by the mass of each isotope required for the reference design. The material requirements are tabulated by actual material plate type for each core region. In addition, the total requirements and the total available inventory are listed. In the column under "Material", 1/4-Na refers to 1/4-inch-thick sodium plates. These plates come in various lengths. The requirements, however, are listed as total linear inches. Based on the proposed core design, there are no inventory requirements beyond the current ZPR/ZPPR materials inventory. This takes into account the possibility of a relatively large critical-assembly program on ZPPR in parallel with the safety-related criticals program on ZPR-9. The requirement for depleted uranium, sodium, uranium oxide and iron oxide represent only a small fraction of the available inventory. There are two columns of plutonium alloy plates in the core unit cell. One column contains 1/4-inch DOW plates and the other contains 1/4-inch SEFOR plates. The DOW plates offer no inventory problems. There is a limited quantity of the SEFOR plates, and it is planned to use about 92% of the available inventory. It appears that the entire inventory of the SEFOR plates can be made available for this program, however. The requirements for sodium-void cans (VDC) are listed in Table XIII. These are needed to simulate sodium voiding in the meltdown sequence steps. The supply of sodium void cans is more than adequate also.

Work on development of the initial program plan listing specific configurations and measurements is in progress and will be included in the next quarterly.

TABLE XI. Isothermal Doppler Reactivity Effect (300-3000°K) for the Step 1 (Reference) and Step 5 (Slumped Fuel) Configurations

	Configuration	k	$\delta k_{Doppler}$
Step 1.	Reference Core, T = 300°K	1.00000	
Step 1.	Reference Core, T = 3000°K for all heavy resonance absorbers throughout core	0.99277	-0.00723
Step 1.	Reference Core, T = 3000°K for ^{238}U only throughout core	0.99223	-0.00777
Step 5.	Slumped Fuel Configuration, T = 300°K	1.00000	
Step 5.	Slumped Fuel Configuration, T = 3000°K for all heavy resonance absorbers throughout core	0.99538	-0.00462
Step 5.	Slumped Fuel Configuration, T = 3000°K for ^{238}U only throughout core	0.99468	-0.00532
Step 5.	Slumped Fuel Configuration, T = 3000°K for ^{238}U only in slumped fuel region only	0.99720	-0.00280

TABLE XII. Sodium-Void Can Requirements and Material Inventory, Linear Inches

	50 Drawer Case			74 Drawer Case			
Material	Core	Axial Blanket	Total	Core	Axial Blanket	Total	Inventory
1/4-VDC	1800	-	1800	2664	-	2664	37964
1/2-VDC	900	1600	2500	1332	2368	3700	36427

TABLE XIII. Material Requirements and Material Inventory, Linear Inches

Material	Core (440 Drawers)	Blanket		Total	Inventory[a]
		Axial (440 Drawers)	Radial (1090 Drawers)		
1/4-Na	15840	-	-	15840	268357 (h) 45035 (m) 38904 (ℓ)
1/2-Na	7920	14080	74120	96120	340777 (h) 86012 (m)
1/8-Fe_2O_3	31680	-	-	31680	139596 (h) 147147 (ℓ)
1/4-U_3O_8	-	21120	111180	132300	499829
1/8-SST	-	7040	37060	44100	174527
1/8-DU	-	7040	37060	44100	915456
1/4-Pu/DU/Mo	7920	-	-	7920	23546 (DOW) 68589 (NUMEC)
1/4-SEFOR	7920	-	-	7920	8576

[a]The letters h, m, and ℓ stand for heavy, medium, and light variations of the material type.

REFERENCES

1. Preliminary Safety Analysis Report, Clinch River Breeder Reactor Project, Project Management Corporation, Oak Ridge, Tennessee.

2. Clinch River Breeder Reactor Plant Nuclear Island Demo Plant Simulation Model (DEMO), WARD-D-0005, Rev. 3, April 1975, Westinghouse Advanced Reactors Division, Madison, Pennsylvania.

3. Physics of Reactor Safety, Quarterly Report, January—March 1975, ANL-75-31, pp. 10-12.

4. N. C. Paik, R. A. Doncals and J. A. Lake, Fuel and Blanket Management for the Clinch River Breeder Reactor, Advanced Reactors: Physics, Design and Economics, Proceedings of the International Conference, Atlanta, Georgia, September 8-11, 1974, p. 677, Pergamon Press, New York (1975).

5. B. J. Toppel and H. Henryson, II, "Methodology and Application of the MC^2-2/SDX Cross-Section Capability," Trans. Am. Nucl. Soc., 16, 126 (1973).

6. W. M. Stacey, et al., "A New Space-Dependent Fast Neutron Multigroup Cross-Section Preparation Capability," Trans. Am. Nucl. Soc., 15, 292 (1972).

7. J. A. Lake, private communication, Westinghouse Advanced Reactors Division, Madison, Pennsylvania.

8. A. M. Broomfield, et al., "The Mozart Control Rod Experiments and Their Interpretation," Proceedings of the International Symposium on Physics of Fast Reactors, October 16-19, 1973, Volume 1, p. 312, Tokyo, Japan.

9. W. R. Bohl, et al., "An Analysis of Transient Undercooling and Transient Overpower Accidents Without Scram in the Clinch River Breeder Reactor," ANL/RAS 75-29, Internal Memorandum, Reactor Analysis and Safety Division, Argonne National Laboratory (July 1975).

10. P. Benoist, "Streaming Effects and Collision Probabilities in Lattices," Nucl. Sci. Eng. 34, 285 (1968).

11. Richard Lell, private communication.

12. Physics of Reactor Safety, Quarterly Report, October—December 1975, ANL-76-13, p. 8.

13. H. U. Wider, "An Improved Analysis of Fuel Motion During an Overpower Excursion," Ph.D. Thesis, Northwestern University, June 1974.

14. M. W. Evans and F. H. Harlow, "The Particle-in-Cell Methods for Hydrodynamic Calculations," LA-2139 (1957).

15. C. W. Hirt et al., "SOLA, A Numerical Solution Algorithm for Transient Fluid Flows," LA-5852, April 1975.

16. C. L. Beck et al., "Streaming Effects in the Analysis of Sodium Void Measurements in ZPPR," Trans. Am. Nucl. Soc. 23 (1976) (to be published).

17. P. I. Amundson, private communication (Dec 30, 1975).

18. P. I. Amundson, private communication (Feb 27, 1976).

19. P. I. Amundson, private communication (Jan 30, 1976).

20. R. A. Harris, "Sodium Void Reactivity Worth in the FTR," HEDL-TME-74-31, July 1974.

21. H. K. Fauske, "Boiling Flow Regime Maps in LMFBR HCDA Analysis," Trans. Am. Nucl. Soc. 22, 385.

22. Physics of Reactor Safety, Quarterly Report, October—December 1975, ANL-76-13, p. 4.

23. P. J. Berenson, "Film Boiling Heat Transfer from a Horizontal Surface," J. Heat Transfer, p. 351 (Aug 1961).